

**Computational Fluid Dynamics analysis of Rectangular  
Microchannel Heat sink**

*A Major Thesis Submitted in Partial Fulfillment of the requirements for the  
award of the degree of*

**Master of Technology**

**In**

**Thermal Engineering**



*Submitted by:*

**Subodh Chandra**  
(2K15/THE/15)

**SESSION 2015-17**

*Under the guidance of*  
**Dr. B.B. Arora**

**Department of Mechanical Engineering**  
**DELHI TECHNOLOGICAL UNIVERSITY,**  
Shahbad Daultapur, Main Bawana Road, Delhi - 42

## DECLARATION

I hereby declare that the work which being presented in the major thesis entitled **“Computational Fluid Dynamics analysis of Rectangular Microchannel Heat sink”** in the partial fulfilment for the award of the degree of Master of Technology in **“Thermal Engineering”** submitted to Delhi Technological University (Formerly Delhi College of Engineering), is an authentic record of my own work carried out under the supervision of **Dr. B. B. ARORA**, Department of Mechanical Engineering, Delhi Technological University (Formerly Delhi College of Engineering). I have not submitted the matter of this dissertation for the award of any other Degree or Diploma or any other purpose what so ever.

Place:

**SUBODH CHANDRA**

Date:

**2K15/THE/15**

## **CERTIFICATE**

This is to certify that **SUBODH CHANDRA**, (2K15/THE/15), student of M.Tech, “THERMAL ENGINEERING”, Delhi Technological University, has submitted the dissertation titled “**Computational Fluid Dynamics analysis of Rectangular Microchannel Heat sink**” towards the partial fulfillment of the requirements for the award of the degree of Master of Technology under my guidance and supervision.

**DR. B. B. ARORA**

Department of Mechanical Engineering

Delhi Technological University

(Formerly Delhi College of Engineering)

Delhi-110042

## **ACKNOWLEDGEMENT**

It is said that gratitude is a virtue. This part is dedicated to special thanks that I would like to deliver to the people who helped me in making the fulfilment of this thesis project possible.

I take great pride in expressing my unfeigned appreciation and gratitude to my learned mentor **DR. B. B. ARORA**, and Department of Mechanical Engineering, Delhi Technological University (Formerly Delhi College of Engineering), for their invaluable inspiration, guidance and continuous encouragement throughout this project work. His critics and suggestions on my work have always guided me towards perfection. This work is simply the reflection of his thoughts, ideas, concepts and above all his efforts. Working under his guidance has been a privilege and an excellent learning experience that I will cherish for a long time.

I express my deepest gratitude to **PROF. R.S. MISHRA**, Head of Department Mechanical Engineering Delhi Technological University (Formerly Delhi College of Engineering). Lastly, I would like to thank my friends **Mr. CHINMAY JAIN**, **Mr. ASHUTOSH MISHRA** and **Mr. TSEWANG TAMCHOS** who helped me a lot.

**SUBODH CHANDRA**

**2K15/THE/15**

# **Computational Fluid Dynamics analysis of Rectangular Microchannel Heat sink**

## **ABSTRACT**

In the study, the analysis of fluid flow and heat transfer in a rectangular microchannel heat sink has been carried out with the help of computational fluid dynamics (CFD). The experimental work done performed by Lee and Mudawar (2002) was simulated for this study. The CFD model equations are solved to analyze the hydrodynamic and thermal behaviour of the rectangular microchannel heat sink. The geometry of the problem is created in Solidworks while meshing has been done in ANSYS Workbench. The model has been solved by ANSYS Fluent 15 solver.

The three-dimensional heat transfer characteristics of the heat sink were analyzed numerically by solving the conjugate heat transfer problem involving simultaneous determination of the temperature distribution in both the solid and liquid regions. The measured pressure drop and temperature distributions show good agreement with the corresponding numerical results. These findings demonstrate that the conventional Navier–Stokes and energy equations can adequately predict the fluid flow and heat transfer characteristics of micro-channel size used in present study.

**Key Words:** *Microchannels, CFD, Fluent, Temperature distribution, pressure drop*

# CONTENT

<b>DECLARATION</b>	<b>I</b>
<b>CERTIFICATE</b>	<b>II</b>
<b>ACKNOWLEDGEMENT</b>	<b>III</b>
<b>ABSTRACT</b>	<b>IV</b>
<b>CONTENT</b>	<b>V</b>
<b>LIST OF FIGURES</b>	<b>VII</b>
<b>LIST OF TABLES</b>	<b>VIII</b>
<b>INTRODUCTION</b>	<b>1</b>
<b>1.1 MICROCHANNEL CONCEPT AND EARLY WORK</b>	<b>3</b>
<b>1.2. FLOW CHANNEL CLASSIFICATION</b>	<b>3</b>
<b>1.3 INTRODUCTION OF COMPUTATIONAL FLUID DYNAMICS (CFD)</b>	<b>5</b>
<b>1.4 AIM OF THE PRESENT WORK</b>	<b>6</b>
<b>1.5 OUTLINE OF THE PROJECT REPORT</b>	<b>7</b>
<b>LITERATURE REVIEW</b>	<b>8</b>
<b>COMPUTATIONAL FLUID DYNAMICS- THEORY AND MODEL EQUATIONS</b>	<b>19</b>
<b>3.1 MATHEMATICAL FORMULATION: GOVERNING EQUATIONS</b>	<b>20</b>
3.1.1 MASS CONSERVATION EQUATION	20
3.1.2 MOMENTUM CONSERVATION EQUATION	20
3.1.3 ENERGY EQUATION	21
<b>3.2 BOUNDARY CONDITIONS</b>	<b>21</b>
<b>3.3 TECHNIQUES FOR NUMERICAL DISCRETIZATION</b>	<b>23</b>
3.3.1 THE FINITE DIFFERENCE METHOD	23

<b>3.3.2 THE FINITE ELEMENT METHOD</b>	<b>23</b>
3.3.3 THE FINITE VOLUME METHOD	23
3.3.4 SPECTRAL METHODS	23
<b><u>MICROCHANNEL HEAT SINK-THEORY, MODEL EQUATIONS AND FABRICATION TECHNOLOGY</u></b>	<b>24</b>
<b>4.1 WHY MICROCHANNEL?</b>	<b>24</b>
<b>4.2 MICROCHANNEL HEAT SINK- MODEL EQUATIONS</b>	<b>25</b>
4.2.1 HEAT TRANSFER IN MICROCHANNELS	26
<b>4.3 METALLIC MICROCHANNEL HEAT SINK</b>	<b>28</b>
<b>4.4 FABRICATION OF MICROCHANNELS</b>	<b>28</b>
4.4.1 PHOTOLITHOGRAPHY:	28
4.4.2 Anisotropic Wet Etching	29
4.4.3 ANISOTROPIC DRY ETCHING	29
4.4.4 DRIE AND RIE (REACTIVE ION ETCHING):	30
4.4.5 FABRICATION OF MICROCHANNELS IN COPPER	30
4.4.5.1 Laser Micromachining	30
4.4.5.2 Focused Ion Beam Milling	30
4.4.5.3 Micro Electro discharge Machining (Micro EDM)	31
<b><u>MODELING OF FLUID FLOW IN RECTANGULAR MICROCHANNEL</u></b>	<b>32</b>
<b>5.1 PROBLEM DESCRIPTION</b>	<b>33</b>
<b>5.2 DETAILED GEOMETRY OF COMPUTATIONAL DOMAIN</b>	<b>34</b>
5.3 MESHING OF COMPUTATIONAL DOMAIN	36
<b>5.4 PHYSICAL MODEL</b>	<b>37</b>
<b>5.5 MATERIAL PROPERTIES</b>	<b>37</b>
<b>5.6 GOVERNING EQUATIONS</b>	<b>37</b>
<b>5.7 BOUNDARY CONDITIONS</b>	<b>38</b>
<b>5.8 METHOD OF SOLUTION</b>	<b>39</b>
<b><u>RESULTS AND DISCUSSIONS</u></b>	<b>40</b>
<b><u>CONCLUSIONS</u></b>	<b>55</b>
<b><u>REFERENCES</u></b>	<b>56</b>

## List of figures

Fig.3.1 Various Boundary conditions -----	22
Fig. 4.1 Schematic representation of Microchannel heat sink -----	25
Figure5.1 Experimental arrangements for testing of micro channel -----	32
Figure 5.2 (a) Test module (b) Microchannel heat sink -----	33
Figure 5.3 a) unit cell b) computational domain -----	35
Figure 5.4 Isometric view of computational domain in Ansys -----	35
Figure 5.5 Isometric view of mesh structure in computational domain -----	36
*Figure 6.1 Temperature distribution at bottom wall of Heat sink at $q_{eff} = 100 \text{ W/cm}^2$ and Re of 890 -----	43
*Figure 6.2 Temperature distribution at Top wall of Heat sink at $q_{eff} = 100 \text{ W/cm}^2$ and Re of 890 -----	43
*Figure 6.3 Temperature distribution at Channel bottom wall of Heat sink at $q_{eff} = 100 \text{ W/cm}^2$ and Re of 890 -----	44
*Figure 6.4 Temperature distribution at Channel side wall of Heat sink at $q_{eff} = 100 \text{ W/cm}^2$ and Re of 890 -----	44
Figure 6.5 Velocity contours in complete fluid domain at $q_{eff} = 100 \text{ W/cm}^2$ and Re of 890 -----	45
Figure 6.6 Velocity contours nearer to inlet at $q_{eff} = 100 \text{ W/cm}^2$ and Re of 890 -----	45
Figure 6.7 Velocity contours nearer to outlet at $q_{eff} = 100 \text{ W/cm}^2$ and Re of 890 -----	46
Figure 6.8 Pressure contours nearer to inlet at $q_{eff} = 100 \text{ W/cm}^2$ and Re of 890 -----	46
Figure 6.9 Pressure contours nearer to outlet at $q_{eff} = 100 \text{ W/cm}^2$ and Re of 890 -----	47
Figure 6.10 Temperature contours of complete heat sink at symmetry plane at $q_{eff} = 100 \text{ W/cm}^2$ and Re of 890 -----	47
*Figure 6.11 Temperature distributions at bottom wall of Heat sink at $q_{eff} = 200 \text{ W/cm}^2$ and Re of 864 -----	48
*Figure 6.12 Temperature distributions at top wall of Heat sink at $q_{eff} = 200 \text{ W/cm}^2$ and Re of 864 -----	48
*Figure 6.14 Temperature distribution at Channel side wall of Heat sink at $q_{eff} = 200 \text{ W/cm}^2$ and Re of 864 -----	49
*Figure 6.13 Temperature distribution at Channel bottom wall of Heat sink at $q_{eff} = 200 \text{ W/cm}^2$ and Re of 864 -----	49
Figure 6.15 Velocity contours in entire fluid domain at $q_{eff} = 200 \text{ W/cm}^2$ and Re of 864 -----	50
Figure 6.16 Velocity contours nearer to inlet at $q_{eff} = 200 \text{ W/cm}^2$ and Re of 864 -----	50



Figure 6.17 Velocity contours nearer to inlet at $q_{eff} = 200 \text{ W/cm}^2$ and Re of 864	51
Figure 6.18 Pressure contours nearer to inlet at $q_{eff} = 200 \text{ W/cm}^2$ and Re of 864	51
Figure 6.19 Pressure contours nearer to inlet at $q_{eff} = 200 \text{ W/cm}^2$ and Re of 864	52
Figure 6.20 Temperature contours of complete heat sink at symmetry plane at $q_{eff} = 200 \text{ W/cm}^2$ and Re of 864	52
Figure 6.21 Graph between Pressure drop and Reynolds Number	53
Figure 6.22 energy balance predictions for water temperature rise from heat sink inlet to outlet: (a) $q_{eff} = 100 \text{ W/cm}^2$ , (b) $q_{eff} = 200 \text{ W/cm}^2$ .	53
Figure 6.23 Graph between friction factor and Reynolds Number	54

### List of tables

Table 1.1	4
Table 1.2	4
Table 4.1 Nusselt No. For Various Geometries	27
Table 5.1 Dimensions of unit cell micro channel	34
Table 5.2 Dimensions of computational domain	34
Table 5.3 Material Properties	37
Table 5.4. Zonewise Boundary Condition	38
Table 5.5 Relaxation factor	39

# CHAPTER- 1

## INTRODUCTION

Heat is an unavoidable by product of any electronic device or mechanical heat engine. The aim of every thermal engineer is to minimize this heat or remove this heat from its source. The efficient removal of this heat is referred as thermal management. This heat sink is the device which is used for sinking away the heat dissipated in the engine or any other device. In case of high heat flux generating electronics device, the miniaturize sizes of these heat generating devices and the strict operating conditions creates a challenging situation to efficiently remove the heat produced. The rapid increase in IC speeds, functionality and miniaturization of devices has fueled an extraordinary acceleration in chip heat dissipation and consequently thermal management is becoming a critical bottleneck to system performance.

The Increase in the temperature of semiconductor devices leads to change in various device parameters. For example, in case of Laser diodes, the threshold current (current at which lasing action starts) of the device increases exponentially with the rise in its junction temperature while the slope efficiency of device decreases exponentially with temperature. Apart from this, the reliability of a laser diode is strongly affected by the temperature rise in the active region as the operating lifetime of the device decreases exponentially with temperature. The failure rate of a semiconductor device follows the Arrhenius equation[1]:

$$F=A(e^{-E_a/kT}) \quad 1.1$$

F: Failure rate

A: Arrhenius constant

T: Junction Temperature (K)

Ea: Activation energy (eV)

K: Boltzmann's constant ( $8.63 \times 10^{-5}$  eV/K)

The failure rate of a component almost doubles with an increase of  $10^\circ\text{C}$  (for an Ea of 0.65 eV).

To efficiently remove the heat dissipated from semiconductor devices, micro-machining technology is the current trend which is gaining popularity for the development of highly efficient cooling systems for semiconductor devices. Microchannel cooling is a technology dealing with very small fins that are placed extremely close to the heat dissipating element. Microchannel heat sink is a device which has the ability to remove very high heat flux with minimum temperature rise.

The need for miniaturized scale channels emerges from the way that for a constant temperature difference the heat exchange rate is proportional to the result of the overall heat transfer coefficient U and the heat exchange region A. The higher increment in UA can be accomplished by expanding the overall heat transfer coefficient U which can be raised by expanding the film heat transfer coefficient h. For flow through pipes and tubes, huge increment in h can be accomplished by reducing hydraulic diameter. That is the reason; microchannel heat sinks can disseminate a lot of heat with least rise in temperature. The small size of microchannel heat sink additionally makes them perfectly suited for cooling the space obliged electronic gadgets.

The two essential targets in semiconductor chip thermal management are the lessening of the gadget's most extreme temperature and the minimization of thermal resistance of the packaged device. Microchannel heat sinks can efficiently accomplish these goals.

In literature, it is mentioned that microchannel heat sinks can remove heat flux of the order of  $1000 \text{ W/cm}^2$  with most extreme surface temperatures of under  $120^\circ\text{C}$  [2]. The likelihood of accomplishing this level of heat flux removal has brought about various reviews for using microchannel flow for the thermal management of high heat flux

generating electronics frameworks. Many of these examinations concentrated on knowing the essentials of fluid flow inside a microchannel. Some examination was centered around looking into the flow and heat transfer attributes in microchannels and in customary channels. Hypothetical examination prompting improvement of microchannel heat sinks were done; so additionally were test examinations to acquire new connections and to augment the scope of use of conventional channel relationships to incorporate in case of microchannels.

The investigation of heat transfers and movement of fluid these channels, which are two basic areas of interest, have pulled in more considerations with wide applications in many applications. Microchannel heat sinks are characterized into two types. First is single-phase in which; fluid does not change its phase. In second type; which is known as two phase microchannel heat sink, fluid gets vaporized (due to low fluid velocity and high heat flux).

### **1.1 Microchannel concept and early work**

The goal of every thermal designer is to get the cooling fluid as close as possible to the heat source. To achieve this, liquid flow through microchannels was firstly shown as an effective method for dispersing heat from silicon incorporated device by Tuckerman and Pease (1981) [3]. The original thought prompted various imaginative plans and generated various research activities in the field of microchannel cooling. This exhibition included the testing of an extremely narrow water-cooled heatsink. Minute channels of 50  $\mu\text{m}$  width and 300  $\mu\text{m}$  of depth carved on silicon, and demineralized water was pumped inside these narrow passages as the coolant. It could expel heat flux of 790  $\text{W}/\text{cm}^2$  and a comparing substrate temperature increase of 71°C above the inlet water temperature. Before continuing with microchannel heat exchange and fluid flow behaviour, it is suitable to present a definition for the expression "microchannel".

### **1.2. Flow channel classification**

Hydraulic diameter can serve the basis of defining microchannel in case of channel is not circular. Mehendale et al. (2000) [4] gave the following basis for the definition of microchannel on the basis of least channel dimension "D" as shown in table 1.1.

**Table 1.1**

$1\ \mu m < D < 100\ \mu m$	:	Microchannels
$100\ \mu m < D < 1\ mm$	:	Minichannels
$1\ mm < D < 6\ mm$	:	Compact Passages
$6\ mm < D$	:	Conventional Passages

Kandlikar (2003) [5] adopted a different classification which has the same basis for its classification i.e. lowest channel dimension “D”. It is given in table 1.2.

**Table 1.2**

$1\ \mu m < D < 10\ \mu m$	:	Transitional Microchannels
$10\ \mu m < D < 200\ \mu m$	:	Microchannels
$200\ \mu m < D < 3\ mm$	:	Minichannels
$3\ mm < D$	:	Conventional Passages

A more straightforward arrangement was proposed by Obot (2003) [6] in view of the hydraulic diameter. Obot arranged channels of hydraulic diameter less than 1 mm ( $D_h < 1\ mm$ ) as microchannels, which is likewise received by numerous different scientists, for example, Bahrami and Jovanovich (2006) [7] and Bayraktar and Pidugu (2006) [8]. This classification is supposed to be most suitable for the reasons for this proposition.

Microchannel heat sinks work on the technology which is capable of transferring high amount of heat flux which is generated inside small area of semiconductor device during its operation. These heat sinks are normally fabricated by using copper in case of metallic microchannel heat sink which has high thermal conductivity among metals. Few experiments were also carried out using CVD (chemically vapour deposited) diamond as microchannel heat sink material. Silicon is material which is preferred while microchannel heat sink to be produced from semiconductor material itself. The microchannels are fabricated by either micro machining technology in case of metals or well established semiconductor fabrication technology when silicon is used as material for microchannel.

A large number of parallel channels in micron range constitute a microchannel heat sink. The shapes are generally circular or rectangular. The coolant which is normally deionised water or water with nanoparticles; is forcefully passed inside these channels to remove heat from heat dissipating device.

Microchannel heat sinks have very high surface area to volume ratio and large convective heat transfer coefficient (comparable to boiling in some cases). Additionally, they possess low mass, small volume and small cooling fluid requirement. These properties make them a good choice for thermal management of semiconductor devices such as semiconductor laser arrays, high speed microprocessors etc.

### **1.3 INTRODUCTION OF COMPUTATIONAL FLUID DYNAMICS (CFD)**

It will be very expensive and time consuming process if all the work on microchannel heat sink is done practically. To diminish the quantity of trials that should be performed, analysts utilize Computational Fluid Dynamics (CFD) as an instrument for heat exchange investigation. CFD can be utilized as a part of parallel with trial setups with an end goal to anticipate the stream and heat exchange qualities of given surface under the predetermined control parameters. Computational techniques can abbreviate the outline cycle and in this way diminish exploratory expenses. Numerical strategies are widely used to break down the liquid conduct, execution and to plan the microchannels warm sink.

Computational Fluid Dynamics (CFD) is software which is a set of numerical algorithms that is used to analyze the fluid flow and heat exchange. Arrangements of mathematical model conditions are first created taking after conservation laws. These conditions are then explained utilizing software so as to get the flow parameters all through the computational area. Validation of CFD results is necessary to evaluate the precision of the CFD analysis. The validation is accomplished by contrasting CFD comes about and accessible exploratory, hypothetical, or explanatory information. Validated models end up plainly settled as dependable, while those which come up short the approval test should be adjusted and revalidated. Additionally, demonstrate conditions can be simulated by CFD technique for the design and development of microchannel heat sink.

#### **1.4 AIM OF THE PRESENT WORK**

The investigation of fluid flow and heat exchange analysis in microchannels is essential for the innovation purpose and to optimize its geometry and flow parameters. The advancements are taking after the pattern of scaling down in all fields. The researches demonstrate that the microchannels and micro fluidics are considered widely for high heat flux applications. However, there is constrained research identified with the execution investigation of micro fluidic devices by utilizing CFD. Taking after from the experimental examination of Lee and Mudawar (2002), this study concentrates on the outcome of CFD analysis of microchannel fluid flow and heat exchange, in a rectangular microchannel heat sink.

The aim of present work is

- Computational Fluid Dynamics analysis of rectangular microchannel heat sink to comprehend its hydrodynamic and thermal nature.
- Validation of the CFD models by contrasting the present results with the experimental work of Lee and Mudawar (2002).

## **1.5 OUTLINE OF THE PROJECT REPORT**

Chapter 1: Detailed introduction of project work with focus on importance of thermal management in semiconductor technology, classification of micro channel, its importance in high heat flux cooling and use of CFD in microchannel heat sink analysis.

Chapter 2: Covers detailed literature review on experimental and theoretical analysis of the microchannel heat sink.

Chapter 3: Explains theory and modeling equation of CFD analysis.

Chapter 4: Describes theory and modeling equation of micro channel heat sink. The fabrication technology of microchannel heat sink is also described in this section briefly.

Chapter 5: Describes modeling of Rectangular microchannel heat sink in detail. The various parts in simulation like geometry, meshing, boundary conditions, Temperature and Pressure variation inside microchannel are described in this section.

Chapter 6: Results and discussions

Chapter 7: Conclusion



## CHAPTER- 2

### LITERATURE REVIEW

A lot of experimental and theoretical work on microchannel heat sink has been done in the last decades. Both the industrial and academic people have taken interest in this area. The following is a review of the research that has been completed on microchannel heat sink. The literature survey is arranged according to similarity to the work done in this thesis. In this literature review emphasis is directed on:

- (a). Experimental study of fluid flow and heat transfer in micro channels
- (b). Numerical study of fluid flow and heat transfer in micro channels

### 2.1 EXPERIMENTAL STUDY OF FLUID FLOW AND HEAT TRANSFER IN MICRO CHANNELS

With the development of micro fabrication technology, microfluidic systems have been increasingly used in different scientific disciplines such as biotechnology, physical and chemical sciences, electronic technologies, sensing technologies etc. Microchannels are one of the essential geometries for microfluidic systems; therefore, the importance of convective transport phenomena in microchannels and microchannel structures has increased dramatically. In recent years, a number of researchers have reported the heat transfer and pressure drop data for laminar and turbulent liquid or gas flow in microchannels.

The concept of micro channel heat sink was first proposed by **Tuckermann and Pease (1981) [3]**, they demonstrated that the micro channel heat sinks, consisting of micro rectangular flow passages, have a higher heat transfer coefficient in laminar flow regime than that in turbulent flow through conventionally-sized devices. They said that the heat transfer can be enhanced by reducing the channel height down to micro scale. This pioneering work initiated other studies, some confirmed findings reported by others. Many researchers compared their numerical or analytical studies with Tuckerman and Pease.

**Wang and Peng (1995) [9]** had investigated experimentally the single-phase forced convective heat transfer characteristics of water/methanol flowing through micro-channels with rectangular cross section of five different combinations, maximum and minimum channel size varying from  $(0.6 \times 0.7 \text{ mm}^2)$  to  $(0.2 \times 0.7 \text{ mm}^2)$ . The results provide significant data and considerable insight into the behavior of the forced-flow convection in micro-channels.

**Peng and Peterson (1996) [10]** had also investigated experimentally the single-phase forced convective heat transfer micro channel structures with small rectangular channels having hydraulic diameters of 0.133–0.367 mm and distinct geometric configurations. The results indicate that geometric configuration had a significant effect on single-phase convective heat transfer and flow characteristics. The laminar heat transfer found to be dependent upon the aspect ratio i.e. the ratio of hydraulic diameter to the centre to centre distance of microchannels. The turbulent flow resistance was usually smaller than predicted by classical relationships.

**Fedorov and Viskanta (2000) [11]** developed a three dimensional model to investigate the conjugate heat transfer in a micro channel heat sink with the same channel geometry used in the experimental work done by Kawano et al (1998) [12]. This investigation indicated that the average channel wall temperature along the flow direction was nearly uniform except in the region close to the channel inlet, where very large temperature gradients were observed. This allowed them to conclude that the thermo-properties are temperature dependent. The modifications of thermo-physical properties in the numerical process are very difficult as temperature and velocity are highly coupled.

**Jiang et al. (2001) [13]** performed an experimental comparison of microchannel heat exchanger with microchannel and porous media. The effect of the dimensions on heat transfer was analyzed numerically. It was emphasized that the heat transfer performance of the microchannel heat exchanger using porous media is better than using of microchannels, but the pressure drop of the former is much larger.

**Qu and Mudawar (2002) [14]** have performed experimental and numerical investigations of pressure drop and heat transfer characteristics of single-phase laminar flow in  $231 \mu\text{m}$  by  $713 \mu\text{m}$  channels. Deionized water was employed as the cooling liquid

and two heat flux levels, 100 W/cm<sup>2</sup> and 200 W/cm<sup>2</sup>, defined relative to the planform area of the heat sink, were tested. Good agreement was found between the measurements and numerical predictions, validating the use of conventional Navier–Stokes equations for micro channels. For the channel bottom wall, much higher heat flux and Nusselt number values are encountered near the channel inlet.

**Qu and Mudawar (2004) [15]** conducted a three-dimensional fluid flow and heat transfer analysis for a rectangular micro channel heat sink using a numerical method similar to that proposed by both Kawano et al. (1998) , and Fedorov and Viskanta. (2000) This model considered the hydrodynamic and thermal developing flow along the channel and found that the Reynolds number would influence the length of the developing flow region. It was also found that the highest temperature is typically encountered at the heated base surface of the heat sink immediately adjacent to the channel outlet and that the temperature rise along the flow direction in the solid and fluid regions can both be approximated as linear.

**Mishan et al. (2007) [16]** has worked on heat transfer and fluid flow characteristic of a rectangular microchannel experimentally, having water as a working fluid. The experimental results of pressure drop and heat transfer confirm that including the entrance effects, the conventional theory is applicable for water flow through microchannels. They have developed new method for measurement of fluid temperature distribution and it gives the fluid temperature distribution inside the channel.

**Lee and Mudawar (2007) [17]** have done experimental work to explore the micro-channel cooling benefits of water-based nanofluids containing small concentrations of Al<sub>2</sub>O<sub>3</sub>. It was observed that the presence of nanoparticles enhances the single-phase heat transfer coefficient, especially for laminar flow. Higher heat transfer coefficients were achieved mostly in the entrance region of micro-channels. However, the enhancement was weaker in the fully developed region. Higher concentrations also produced greater sensitivity to heat flux. A large axial temperature rise was associated with the decreased specific heat for the nanofluid compared to the base fluid. For two-phase cooling, nanoparticles caused catastrophic failure by depositing into large clusters near the channel exit due to localized evaporation once boiling commenced.

**Chein and Chuang (2007) [18]** have addressed microchannel heat sink (MCHS) performance using nanofluids as coolants. They have carried out a simple theoretical analysis that indicated more energy and lower microchannel wall temperature could be obtained under the assumption that heat transfer could be enhanced by the presence of nanoparticles. The theoretical results were verified by their own experimental results. It was observed that nanofluid-cooled MCHS could absorb more energy than water-cooled MCHS when the flow rate was low. For high flow rates, the heat transfer was dominated by the volume flow rate and nanoparticles did not contribute to the extra heat absorption.

**Jung et al (2009) [19]** have studied experimentally the heat transfer coefficients and friction factor of Al<sub>2</sub>O<sub>3</sub> with diameter of 170 nm in a rectangular micro channel. Appreciable enhancement of the convective heat transfer coefficient of the nanofluids with the base fluid of water and a mixture of water and ethylene glycol at the volume fraction of 1.8 volume percent was obtained without major friction loss. It has been found that the Nusselt number increases with increasing the Reynolds number in laminar flow regime, which is contradictory to the result from the conventional analysis.

**Ergu et al. (2009) [20]** had described the pressure drop and local mass transfer in a rectangular microchannel having a width of 3.70 mm, height of 0.107 mm and length of 35 mm. The pressure drop measurements were carried out with distilled water as working fluid at Reynolds numbers in the range of 100–845, while mass transfer measurements with a chemical solution at Reynolds numbers in the range of 18–552 by using the electrochemical limiting diffusion current technique (ELDCT). Experimental friction factors were found slightly higher than those calculated by theoretical correlation. The Sherwood number correlation was also obtained.

## **2.2 NUMERICAL STUDY OF FLUID FLOW AND HEAT TRANSFER IN MICRO CHANNELS**

To design an effective microchannel heat sink, fundamental understanding of the characteristics of the heat transfer and fluid flow in microchannel are necessary. At the early stages the designs and relations of macroscale fluid flow and heat transfer were

employed. The strength of numerical simulations is the possibility to investigate small details that are impossible to observe in experiments.

**Liu and Garimella (2004) [21]** have studied numerically on fluid flow and heat transfer in microchannels and confirmed that the behavior of micro channels is quite similar to that of conventional channels. And their analysis showed that conventional correlations offer reliable predictions for the laminar flow characteristics in rectangular micro channels over a hydraulic diameter in the range of 244–974  $\mu\text{m}$ .

A numerical study has been performed by **Li et al. (2004) [22]** on the same micro channel heatsink developed by Qu and Mudawar (2000) in order to explore the impact of geometric and thermo-physical parameters of the fluid on its flow behavior and heat transfer characteristics.

The authors have acknowledged the scattered results obtained in past micro fluidics studies from various authors, and pointed out the strong differences of empirical correlations derived therein. These differences are especially true when comparing works that studied single micro channels to those who considered entire micro channel heat sinks. Thus, the authors noted a need to develop numerical models that provide more insight into the fundamental physics of the transport processes involved.

**Roy et al. (2004) [23]** has studied a steady, laminar flow and heat transfer of a nanofluid flowing inside a radial channel between two coaxial and parallel discs. The non-dimensional governing equations of mass, momentum and energy were solved by computational fluid dynamics method. Results presented in this paper are for a water/aluminium oxide particle nanofluid ( $\text{H}_2\text{O}-\gamma \text{Al}_2\text{O}_3$ ). Results have shown that the inclusion of nanoparticles in a traditional coolant can provide considerable improvement in heat transfer rates, even at small particle volume fractions. Increases in the resulting wall shear stresses were also noticed.

**Gamrat et al. (2005) [24]** analyzed three-dimensional flow and associated heat transfer in a rectangular micro channel heat sink numerically. The numerical simulation considered the coupling between convection in micro channels and conduction in the walls and in the complete solid material. The results of numerical simulations using the

continuum model (conventional mass, Navier–Stokes and energy equations) were in good agreement with published data on flow and heat transfer in three dimensional channels.

**Hetsroni et al. (2005) [25]** has verified the capacity of conventional theory to predict the hydrodynamic characteristics of laminar Newtonian incompressible flows in micro channels in the range of hydraulic diameter from  $15 h D$  to  $D m h = 4010 \mu$ . They have compared their results with the data available in open literature. The theoretical models were subdivided in two groups depending on the degree of correctness of the assumptions. The first group includes the simplest one-dimensional models assuming uniform heat flux, constant heat transfer coefficient, etc. The comparison of these models with experiment shows significant discrepancy between the measurements and the theoretical predictions. The second group is based on numerical solution of full Navier–Stokes and energy equations, which account the real geometry of the micro-channel, presence of axial conduction in the fluid and wall, energy dissipation, non adiabatic thermal boundary condition at the inlet and outlet of the heat sink, dependence of physical properties of fluid on temperature, etc. These models demonstrate a fairly well correlation with the available experimental data.

**Khanafer et al. (2003) [26]** has investigated heat transfer enhancement in a two-dimensional rectangular enclosure utilizing nanofluids. The material used is water/copper. The developed transport equations were solved numerically using the finite-volume approach along with the alternating direct implicit procedure. The effect of suspended ultrafine metallic nanoparticles on the fluid flow and heat transfer processes within the enclosure was analyzed. The heat transfer correlation of the average Nusselt number for various Grashof numbers and volume fractions was also presented.

**Jou and Tzeng (2006) [27]** have used the Khanafer's model to analyze heat transfer performance of nanofluids inside an enclosure taking into account the solid particle dispersion. Transport equations were modeled by a stream function-vorticity formulation and solved numerically by finite difference approach. Based upon the numerical predictions, the effects of Rayleigh number (Ra) and aspect ratio on the flow pattern and energy transport within the thermal boundary layer were presented. It was observed that increasing the buoyancy parameter and volume fraction of nanofluids cause an increase in

the average heat transfer coefficient. Finally, the empirical equation was built between average Nusselt number and volume fraction.

**Li and Peterson (2007) [28]** have worked on identification of the possible mechanisms that contribute to the enhanced effective thermal conductivity of nanoparticle suspensions (nanofluids). The mixing effect of the base fluid in the immediate vicinity of the nanoparticles caused by the Brownian motion was analyzed, modeled and compared with existing experimental data available in the literature. The simulation results using CFX 5.5.1 software indicate that this mixing effect can have a significant influence on the effective thermal conductivity of nanofluids. They have found pressure, velocity and temperature profile around the nanoparticles.

A developing laminar forced convection flow of a water–Al<sub>2</sub>O<sub>3</sub> nanofluid in a circular tube, submitted to a constant and uniform heat flux at the wall, has been numerically investigated by Bianco et al. (2009). CFD method was used to simulate the model equations. A single and two-phase model (discrete particles model) was employed with either constant or temperature dependent properties. The maximum difference in the average heat transfer coefficient between single- and two-phase models results was found about 11%. Convective heat transfer coefficient for nanofluids was found as greater than that of the base liquid. Heat transfer enhancement increases with the particle volume concentration, but it is accompanied by increasing wall shear stress values. Higher heat transfer coefficients and lower shear stresses were detected in the case of temperature dependent models. The heat transfer always improves, as Reynolds number increases.

**Xu et al. (2008) [29]** considered liquid flow in 30–344  $\mu\text{m}$  (hydraulic diameter) channels at Reynolds numbers varies from 20 to 4000. Their results showed that characteristics of flow in micro channels agree well with conventional behavior predicted by Navier–Stokes equations. They have suggested that deviations from classical behavior reported in earlier studies may have resulted from errors in the measurement of micro channel dimensions, rather than any micro scale effects.

**Sabbah et al. (2008) [30]** observed that the prediction of heat transfer in micro-channels becomes difficult with increase in complicity of the geometry of the micro-channels, requiring three dimensional analysis of heat transfer in both solid and liquid phases.

Computational Fluid Dynamics (CFD) models were implemented in order to study and optimize the thermal and hydraulic performance of micro channel heat sinks. Despite the small width of the channels, the conventional Navier Stokes and energy conservation equations still apply to the MCHE flow due to the continuum of the working fluid where the channel width is many times larger than the mean free path of liquid molecules (water). The microchannel is characterized by the laminar flow in it, due to the small hydraulic diameter of the channel which results in low Reynolds numbers

**Oztop et al. (2008) [31]** has carried out CFD study on heat transfer and fluid flow due to buoyancy forces in a partially heated rectangular enclosure filled with nanofluids. The temperature of the right vertical wall kept lower than that right wall while other two walls are insulated. The finite volume technique is used to solve the governing equations. Different types of nanoparticles were tested. An increase in mean Nusselt number was found with the volume fraction of nanoparticles for the whole range of Rayleigh number. Heat transfer also increases with increasing of height of heater. It was also found that the heater location affects the flow and temperature fields when using nanofluids.

**Mokrani et al. (2009) [32]** developed a reliable experimental device and adequate methodology to characterize the flow and convective heat transfer in flat micro channels. The study was concerned with measurement of pressure drop and heat transfer by a Newtonian fluid flow inside a flat micro channel of rectangular cross-section whose aspect ratio is sufficiently high that the flow can be considered two dimensional. They considered the hydraulic diameter as twice of the channel height. The mathematical model used to describe the convective heat transfer between the walls and the fluid takes into account the whole field (solid wall and fluid layer) and the coupling between the conduction and the convection modes. Finally, they concluded that the conventional laws and correlations describing the flow and convective heat transfer in ducts of large dimension are directly applicable to the micro channels of heights between 500 and 50 microns

**Muthamilselvan et al. (2009) [33]** has conducted a numerical study to investigate the transport mechanism of mixed convection in a lid-driven enclosure filled with nanofluids. The two vertical walls of the enclosure were kept insulated while the horizontal walls



were at constant temperatures with the top surface moving at a constant speed. The model equations were discretized by finite volume technique with a staggered grid arrangement. The SIMPLE algorithm is used for handling the pressure velocity coupling. Numerical solutions are obtained for a wide range of parameters and copper-water nanofluid was used with  $Pr = 6.2$ . The streamlines, isotherm plots and the variation of the average Nusselt number at the hot wall have been presented and discussed. The variation of the average Nusselt number was observed linear with solid volume fraction.

In one of the recent studies by **Al-Nmir et al. (2009) [34]**, an investigation of the hydrodynamic and thermal behavior of the flow in parallel plate micro heat exchanger was performed numerically, by adopting a combination of both the continuum approach and the possibility of slip at the boundaries. In their work, both viscous dissipation and internal heat generation were neglected. Fluent analysis was made based on solving continuum and slip boundary condition equations. Effects of different parameters; such as, Knudsen number (Kn), heat capacity ratio (Cr), effectiveness ( $\epsilon$ ), and number of transfer units (NTU) were examined. The study showed that both the velocity slip and the temperature jump at the walls increase with increasing Kn. The increase of the slip conditions reduces the frictional resistance of the wall against the flow, and under the same pressure gradient, pumping force leads to that the fluid flows much more in the heat exchanger.

Very recently, **Mathew and Hegab (2009) [35]** theoretically analyzed the thermal performance of parallel flow micro heat exchanger subjected to constant external heat transfer. The model equations predict temperature distributions as well as effectiveness of the heat exchanger. Moreover, the model can be used when the individual fluids are subjected to either equal or unequal amounts of external heat transfer.

One of the comprehensive studies in counter flow micro channel heat exchanger area was done by Hasan et al. 2009. In this work, numerical simulations were made to study the effect of the size and shape of channels; such as circular, square, rectangular, iso-triangular, and trapezoidal, in counter flow exchanger. The results show that for the same volume of heat exchanger, increasing the number of channels leads to an increase in both

effectiveness and pressure drop. Also circular channels give the best overall performance (thermal and hydraulic) among various channel shapes.

**Kang and Tseng (2007) [36]** theoretically modeled thermal and fluidic characteristics of a crossflow micro heat exchanger assuming that flows in rectangular channels, where fin height and width are 32  $\mu\text{m}$  and 200  $\mu\text{m}$  respectively, are incompressible, steady, and laminar. The simulated results were validated with the experimental data. The effects of change of material from copper to silicon and dimensions on its performance were investigated. The study shows that under the same effectiveness value, a small rise in the temperatures of working fluids results in an increase of the heat transfer rate, but a decrease in pressure drop occurs.

Foli et al. (2006) introduced multi-objective genetic algorithms for determining the optimal geometric parameters of the microchannels heat exchanger to maximize the heat transfer rate under specified design constraints. CFD analysis with an analytical method of calculating the optimal geometric parameters was also performed. This paper is important and a good work, because there is limited published literature on attempts at designing the exchanger for optimal performance.

**Tsuzuki et al. (2009) [37]** proposed a new flow configuration, named S-shaped fin configuration to reduce the micro channel heat exchanger pressure drop. A numerical study using a 3DCFD code, FLUENT, was performed to find Nusselt number correlations for the exchanger.

The copper heat exchanger, whose dimensions are 1240 x 68 x 4.75 mm<sup>3</sup>, comprises cold water channels and hot CO<sub>2</sub> channels. For both hot and cold sides, simulations were done to attain accurate empirical correlations for different temperatures.

**Rebrov et al. (2011) [38]** has reviewed the experimental and numerical results on fluid flow distribution, heat transfer and combination thereof, available in the open literature. They have found that the experiments with single channels are in good agreement with predictions using the published correlations. The accuracy of multichannel experiments is lower due to flow maldistribution. Special attention was devoted to theoretical and experimental studies on the effect of a flow maldistribution on the thermal micro reactors.

The review consists of two parts. In the first, the main methods to control flow distribution were reviewed. Several different designs of inlet/outlet chambers were presented together with corresponding models used for optimization of flow distribution. In the second part, recent achievements in understanding of heat transfer in micro channels are presented

**Bachok et al (2011) [39]** has studied numerically a steady flow of an incompressible viscous fluid due to a rotating disk in a nanofluid. The transformed boundary layer equations have been solved numerically by a finite difference scheme, namely the Keller-box method. Numerical results for the flow and heat transfer characteristics were obtained for various values of the nanoparticle volume fraction and suction/injection parameter. Two models for the effective thermal conductivity of the nanofluid, namely the Maxwell-Garnett model and the Patel model, were considered. It was found that for the Patel model, the heat transfer rate at the surface increases for both suction and injection, whereas different behaviours were observed for the Maxwell-Garnett model.

**Allen (2007) [40]** had investigated fluid flow and heat transfer in microchannels experimentally and numerically. Fluid flow and heat transfer experiments were conducted on a copper microchannel heat exchanger with constant surface temperature. The experimentally obtained friction factor were found fairly well agreement with theoretical correlations and moreover the experimental Nusselt number results agreed with theory very well in the transition/turbulent regime, but the results show a higher Nusselt number in the laminar regime than predicted by theoretical correlations. Philips created a CFD model to simulate the fluid in the inlet plenum and the microchannels. The results from these simulations showed good agreement with the experimental data in the transition/turbulent regime as well as with theoretical correlations for laminar and turbulent flow.

## CHAPTER -3

### COMPUTATIONAL FLUID DYNAMICS- THEORY AND MODEL EQUATIONS

Computational fluid dynamics (CFD) is that area of fluid mechanics which uses set of particular numerical algorithms and calculations to tackle and dissect issues which includes flow of fluid. The codes which are used for CFD analysis are well established and along these lines give a decent start to more intricate heat exchanger and fluid flow issues. Application of the CFD for the analysis of a fluid problem is done in these steps.

1. First of all, the mathematical equations which are used to describe the motion of fluid; are written in the form of partial differential equations. After that, these partial equations are discretized.
2. The area of interest in CFD analysis is then assigned as different domains. Now, the domain is divided into several small parts known as grids or elements.
3. In the last, the specific boundary conditions are applied as per the problem for solving the equations.

The solution can be achieved directly or through iteration. Apart from this, a number of control parameters are used to specify convergence and accuracy. All CFD codes consist of following:

- A pre-processor- To input the problem geometry, mesh generation and to set boundary conditions of particular problem.
- A flow solver- To solve the governing equations applied on fluid flow. A flow solver can use following methods:
  - (i) finite element method,
  - (ii) finite difference method;
  - (iii) finite volume method, and
  - (iv) spectral method

- A post-processor- To give the output data and to show the results in graphical manner.

### 3.1 Mathematical formulation: Governing Equations

The governing equations include the equation of continuity, momentum equation and energy equation. The velocity vector is obtained using the continuity and momentum. The energy equation is utilized to get temperature variation at various planes. The governing equations are written here in their general form.

#### 3.1.1 Mass Conservation Equation

The continuity equation is shown below:

$$\frac{\partial \rho}{\partial t} + \nabla \cdot (\rho \vec{v}) = S_m \quad (3.1)$$

Equation (3.1) is the general form of the mass conservation equation. This general form of continuity equation is valid for all kinds of fluid flow; whether it is compressible flow or incompressible. The  $S_m$  represents the additional mass which is added to compensate any loss.

#### 3.1.2 Momentum Conservation Equation

Conservation of momentum equation can be written as:

$$\frac{\partial}{\partial t} (\rho \vec{v}) + \nabla \cdot (\rho \vec{v} \vec{v}) = -\nabla p + \nabla \cdot (\vec{\tau}) + \rho \vec{g} + \vec{F} \quad (3.2)$$

Where

- $p$ -is the static pressure.
- $\vec{\tau}$ -The stress tensor (described below), and
- $\rho \vec{g}$  and  $\vec{F}$  - the gravitational body force and external body forces.

The stress tensor is given by

$$\bar{\tau} = \mu \left[ (\nabla \bar{v} + \nabla \bar{v}^T) - \frac{2}{3} \nabla \cdot \bar{v} I \right] \quad (3.3)$$

Where

- $\mu$  : The molecular viscosity,
- $I$ : The unit tensor and
- The second term on the rightside is the result of volume enhancement.

### 3.1.3 Energy equation

Energy equation in fluent is used in the following form:

$$\frac{\partial}{\partial t} (\rho E) + \nabla \cdot (\bar{v} (\rho E + p)) = \nabla \cdot \left( \kappa_{eff} \nabla T - \sum_j h_j \bar{J}_j + (\bar{\tau}_{eff} \cdot \bar{v}) \right) + S_h \quad (3.4)$$

Where

- $\kappa_{eff}$  is the effective conductivity
- $J_j$  is the diffusion flux of species J and
- The initial three terms on the right-hand side of equation gives energy exchange because of conduction, species dissemination, and viscosity changes, separately.  $S_h$  incorporates the heat of chemical reaction etc.

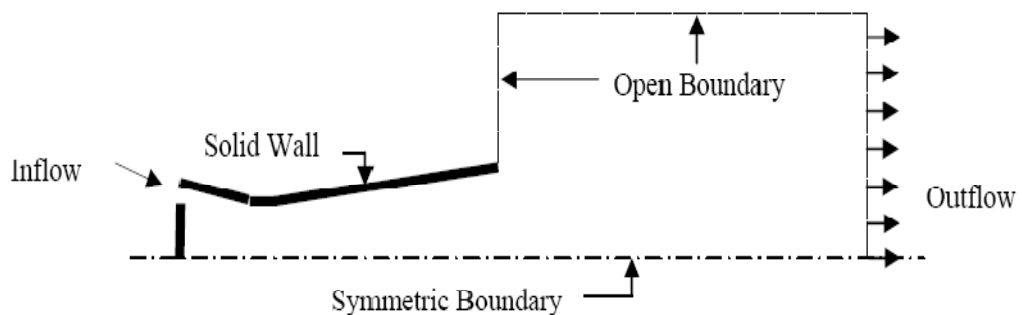
### 3.2 Boundary Conditions

The governing equation of fluid flow may bring about an answer when the boundary conditions and the underlying conditions are indicated. By and large, the boundary conditions are appointed either as the numerical terms. In case of steady state fluid flow, three sorts of boundary conditions are used:

- I. Dirichlet boundary condition
- II. Neuman boundary condition and
- III. Mixed boundary condition

The general boundary condition which are observed in fluid flow are:

- (A) Solid Walls : They can be moving or stationary.
- (B) Inlets: Fluid entrance point.
- (C) Symmetry boundary: Fluid flow is symmetrical about any wall or plane.
- (D) Cyclic boundary: It is in pairs having identical values at some particular place.
- (E) Pressure Boundary Conditions: Identification of pressure boundary condition at one or more than one boundaries is a very important and useful thing. Pressure boundaries are identified by restricted storage of fluid, operational ambience and pressures generated by any mechanical devices.
- (F) Opening Boundary Conditions: Fluid may go out or can enter without any restriction.
- (G) Free Surfaces and Interfaces: Surface tension comes in to play in case of free surfaces..



*Fig.3.1 Various Boundary conditions*

### **3.3 Techniques for Numerical Discretization**

#### **3.3.1 The Finite Difference Method**

Taylor series expansion is used to find out the derivatives of any variable. It is used as the differences between values of the different variable at various locations. 3.3.2 The Finite Element Method

#### **3.3.2 The Finite Element Method**

The fluid domain of interest is divided into several elements. A simple function is assigned for every variable under each element. Then, change in variation is summarized to find flow field.

#### **3.3.3 The Finite Volume Method**

The finite volume method is currently the most used method in CFD. It is also called the Cell Centered (CC) Method. In FVM, the flow governing parameters are assigned at the center of the computational volume.

#### **3.3.4 Spectral Methods**

Fourier series is used to approximate the unknown values.



## CHAPTER-4

### MICROCHANNEL HEAT SINK-THEORY, MODEL EQUATIONS AND FABRICATION TECHNOLOGY

Microchannel heat sinks are composed of very small channels cut through a metal or semiconductor. They can also be considered as small fins that are placed extremely close to the heat dissipating element. These channels have very small hydraulic diameter (in microns' level) which increases film heat transfer coefficient  $h$ , to a very high level. This in turn increases the heat transfer rate which is a key requirement in today's high performing semiconductor devices.

#### 4.1 Why Microchannel?

The heat transfer due to convection is given by:

$$Q = hA(T_{\text{solid}} - T_{\text{liquid}})$$

Thus the heat transferred can be increased either by making

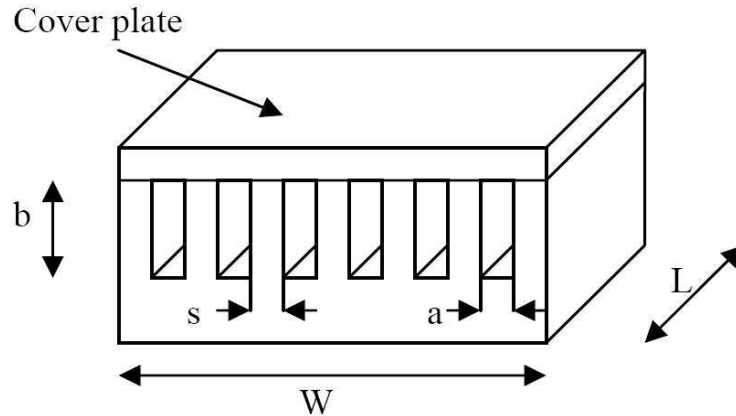
- Area "A" larger
- Heat transfer coefficient "h" larger or
- Increasing the temperature difference

The heat transfer coefficient  $h$  is given by:

$$h = NuK/D_h \quad 4.1$$

Where  $D_h$  is the hydraulic diameter of the channel and  $Nu$  is the Nusselt number characteristic for the flow. It is clear that for a fixed Nusselt number in a channel flow, heat transfer coefficient can be increased by reducing its hydraulic diameter;  $D_h$ . However the decrease in the diameter results in a very large increase of the pressure drop inside the channel. Thus in applications where the heat flux is large, microchannel heat sink helpsto maximize the convective heat transfer coefficient, and also decrease size and cost.

## 4.2 Microchannel Heat sink- Model Equations



*Fig. 4.1 Schematic representation of Microchannel heat sink*

In the above schematic, width “a” and depth” b” are the main important sides of microchannel heatsink which plays an important role in heat transfer. The channel length “L”is decided on the basis of semiconductor chip dimension. The number of channels is governed by the width of channel “a”. The gap between two channels is referred as wall thickness is shown here as “s”.

The number of channels “n”can be calculated from:

$$n=W/(a+s) \quad (4.2)$$

The hydraulic diameter is derived from:

$$D_h= 4ab/2(a+b) \quad (4.3)$$

The channel aspect ratio is given by:

$$\alpha= b/a \quad (4.4)$$

### 4.2.1 Heat transfer in microchannels

In classical analysis, Nusselt number is assumed to be constant when the flow is in fully developed laminar region. The Nusselt number in above case is fixed and it is dependent upon the channel shape and the heat transfer conditions at the wall from where heat load is applied. Table 4.1 shows the Nusselt numbers for generally utilized shapes with constant wall heat flux and constant wall temperature.

In 1978, Shah and London gave the following relation to a rectangular channel. The short side is designated by “a” and long side “b”. Then channel aspect ratio is defined as;  $\alpha_c = a/b$ .

$$Po = fRe = 24(1 - 1.3553 \alpha_c + 1.9467 \alpha_c^2 - 1.7012 \alpha_c^3 + 0.9564 \alpha_c^4 - 0.2537 \alpha_c^5) \quad (4.5)$$

Po is Poiseuille number.

In case, the geometry of channel is rectangular, the Nusselt number is dependent on the channel aspect ratio  $\alpha_c = a/b$ , and the boundary conditions of wall of heat flux. Depending upon various wall conditions, three types of boundary conditions are specified and Nusselt number in each case is described here.

1. Constant wall temperature, T-boundary condition:

$$Nu_T = 7.541(1 - 2.610\alpha_c + 4.970\alpha_c^2 - 5.119\alpha_c^3 + 2.702\alpha_c^4 - 0.548\alpha_c^5) \quad (4.6)$$

2. Constant circumferential wall temperature, uniform axial heat flux, H1 boundary condition:


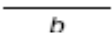
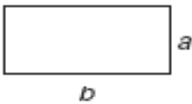


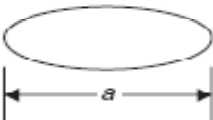
$$Nu_{H1} = 8.235(1 - 2.0421\alpha_c + 3.0853\alpha_c^2 - 2.4765\alpha_c^3 + 1.0578\alpha_c^4 - 0.1861\alpha_c^5) \quad (4.7)$$

3. Constant wall heat flux, both circumferentially and axially:

$$Nu_{H2} = 8.235(1 - 10.6044\alpha_c + 61.1755\alpha_c^2 - 155.1803\alpha_c^3 + 176.9203\alpha_c^4 - 72.9236\alpha_c^5) \quad (4.8)$$

**Table 4.1 Nusselt No. For Various Geometries**

Fanning friction factor and Nusselt number for fully developed laminar flow in ducts, derived from Kakac *et al.* (1987).

Duct shape		$Nu_H$	$Nu_T$	$Po = fRe$	
	Circular	4.36	3.66	16	
	Flat channel	8.24	7.54	24	
	Rectangular, aspect ratio, $b/a =$	1	3.61	2.98	14.23
		2	4.13	3.39	15.55
		3	4.79	3.96	17.09
		4	5.33	4.44	18.23
		6	6.05	5.14	19.70
		8	6.49	5.60	20.58
	Hexagon	4.00	3.34	15.05	
	Isosceles Triangle, Apex angle $\theta =$	10°	2.45	1.61	12.47
		30°	2.91	2.26	13.07
		60°	3.11	2.47	13.33
		90°	2.98	2.34	13.15
		120°	2.68	2.00	12.74
	Ellipse, Major/Minor axis $a/b =$	1	4.36	3.66	16.00
		2	4.56	3.74	16.82
		4	4.88	3.79	18.24
		8	5.09	3.72	19.15
		16	5.18	3.65	19.54

$Nu = hD_h/k$ ;  $Re = \rho u_m D_h/\mu$ ;  $Nu_H$  –  $Nu$  under a constant heat flux boundary condition, constant axial heat flux, and uniform circumferential temperature;  $Nu_T$  –  $Nu$  under a constant wall temperature boundary condition;  $f$  – friction factor.

In actuality, every handy circumstance falls some place amidst these three conditions. This turns into a particularly critical issue on account of microchannels as a result of the trouble in recognizing a suitable condition.

### **4.3 Metallic Microchannel heatsink**

Metallic microchannel heatsink is used to remove the heat generated by high heat flux generating semiconductor devices. The metallic microchannel heatsink is made from several thin sheets. All the metal sheet or laminates which are used for the fabrication purpose is precisely machined with tolerances of the order of approximately 10  $\mu\text{m}$ . Afterwards, these sheets are joined together at high temperature to form the microchannels. Electrolytic or galvanic corrosion and erosion of the internal structure of microchannels are major concern. Deionized water is normally used in microchannel which is used to avoid the electrical connection between the water and the semiconductor device. This deionized water is the main source of this metallic erosion.

Due to this erosion, the small metal particles are dislodged which can block the microstructure. To minimize these effects, a chiller equipped capable of filtering particles below 20  $\mu\text{m}$  is needed.

### **4.4 Fabrication of micro channels**

Single crystal silicon, polycrystalline silicon and metals such as copper are used for the construction of micro channels.

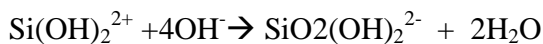
#### **Certain basic processes:**

**4.4.1 Photolithography:** A photosensitive emulsion layer called photoresist, which are used to transfer a pattern through a mask to a semiconductor wafer. A mask is made from a transparent glass plate which is having chromium patterns over them. A process called spin coating is used to deposit a layer of photoresist of the required thickness on silicon. After preparing a mask by the above process, channels can be produced through many processes.

#### 4.4.2 Anisotropic Wet Etching

In this process, the channels are cut using chemical etchants such as Alkali hydroxides (NaOH, KOH, CsOH), ammonium hydroxide, and others like hydrazine and water.

##### Chemical Reaction:



With the use of KOH for anisotropic etching V shaped grooves can be achieved conveniently. Tapered walls in silicon can also be etched through this method.

By Using wafers of different orientation we can get different etch profiles and differently shaped channels. The depth of the channels is controlled by the etching time and the concentration of the etchant.

The channel is covered with a glass or silicon sheet which are joined through Anodic bonding. The dimensions of the channel produced are about 300 micrometers deep and 100 micrometers wide.

#### 4.4.3 Anisotropic Dry Etching

This process allows us to etch high aspect ratio trenches in the silicon wafer. It does not depend on the crystalline orientation of the surface.

It is usually alternated with Chemical vapor deposition which is used to protect the etched surface, for e.g.  $\text{SF}_6$  is deposited to prevent etching of the walls and the bottom etched to give a deeper channel.

#### **4.4.4 DRIE and RIE (Reactive ion etching):**

In DRIE, thin films of two different materials are used. One film as a structural material (commonly polysilicon) and another film is called sacrificial material (oxide). These thin films are deposited and dry etched in an order of sequence. In the last, the second layer which is sacrificial material is wet etched for the release the desired structure.

#### **4.4.5 Fabrication of micro channels in copper**

Copper is another material that is used to make heat sinks due to its high thermal conductivity and can also be used to make micro channels.

##### **4.4.5.1 Laser Micromachining**

Commonly used lasers are:

- 1) Excimer lasers with UV wavelength
- 2) Nd:YAG with infrared and visible and UV wavelength
- 3) CO<sub>2</sub> laser with deep infrared wavelength

In laser machining, very short duration laser pulses are used to remove material. The pulse duration, intensity of laser and optics are decided on the basis of thickness of the material to be removed. A mask is used to remove material from selective region. As, the laser beam can be focused to a very small size, quite complex and narrow dimensions can be achieved.

##### **4.4.5.2 Focused Ion Beam Milling**

In focused ion beam milling also, we can get the spot size as low as 10 nm or even less than that. A beam of energetic ion which is highly focused at the target cuts the particular site of interest.

#### **4.4.5.3 Micro Electro Discharge Machining (Micro EDM)**

In Micro EDM process, sparks are created between electrode (tool) and a workpiece to remove material from material. The spark generates local temperatures as high as 10000°C. This high temperature melts the metal and removes it from site.



## CHAPTER-5

### MODELING OF FLUID FLOW IN RECTANGULAR MICROCHANNEL

In this section, the CFD analysis of fluid flow and heat transfer in a rectangular microchannel is explained. These micro channels are fixed inside test module. The experimental setup was developed by (Qu and Mudawar,2002) which is shown in Fig. 5.1. The details of micro channel test set up are shown in Fig.5.2. (Qu and Mudawar, 2002). These micro channels are fabricated from oxygen free high conductivity copper. The top of heat sink is covered by polycarbonate sheet.

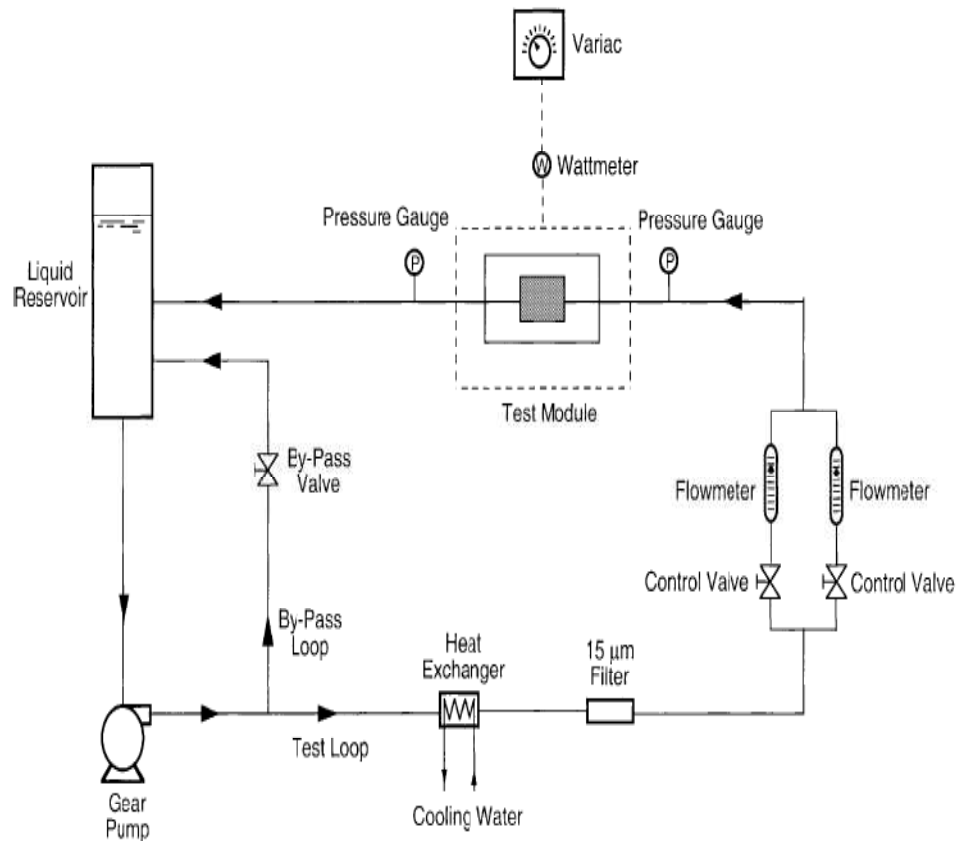


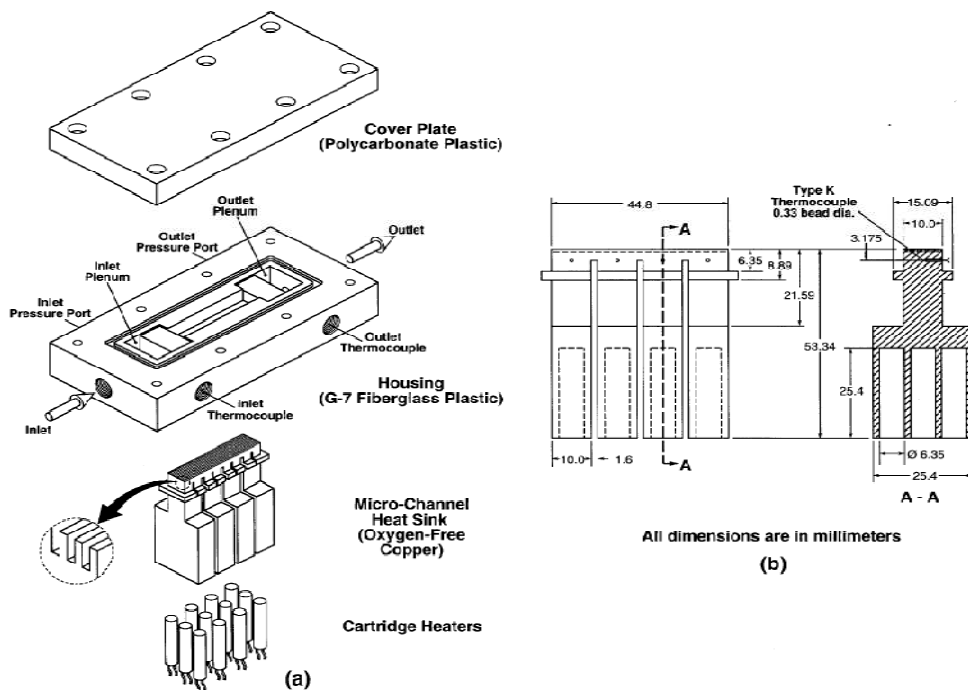
Figure 5.1 Experimental arrangement for testing of micro channel (Qu and Mudawar; 2002)

## 5.1 Problem description

In this work, the simulation is carried out on the experimental set up which was used by Lee and Mudawar, (2002) . Fluid (deionized water) is forced to pass through the rectangular micro channels which are fixed in a test set up. In this work, total 21 micro-channels are there. They all are rectangular in shape and parallel to each other. The sides of a single microchannel unit are as follows:

It is  $231 \mu\text{m}$  in width,  $713 \mu\text{m}$  in depth and  $4.48 \text{ cm}$  long. The hydraulic diameter of microchannel is found to be  $349 \mu\text{m}$ . The inlet velocity is  $u$  (m/s) which depends upon flow rate.

The heat load at the bottom wall is provided by 12 cartridge heaters. These cartridge heaters are fixed inside the bottom wall of heat sink. The polycarbonate top cover plate of heat sink is exposed to convective conditions.



The experiment was carried out at following conditions:

Demineralized water was used as the cooling media and two heat flux of  $q''_{\text{eff}} = 100 \text{ W/cm}^2$  and  $q''_{\text{eff}} = 200 \text{ W/cm}^2$  were applied at the bottom surface (Total area=4.48  $\text{cm}^2$ ) of the heat sink. The Reynolds number range varied from 139 to 1672 in case of  $q''_{\text{eff}} = 100 \text{ W/cm}^2$ , and 385 to 1289 in case of  $q''_{\text{eff}} = 200 \text{ W/cm}^2$ . Inlet temperature of fluid to the channel;  $T_{\text{in}}=15^\circ\text{C}$ .

## 5.2 Detailed geometry of computational domain

In this analysis, half section of a single unit of micro channel istaken as computational domain due to symmetrical nature of microchannel. Figure 5.3 represents the single cell and its half section.i.e. computationaldomain. Isometric view of computational domain (half section of unit cellof micro channel) is also shown in figure 5.4.The dimension of single micro channel and computational domain aregiven in Table 5.1 and Table 5.2 respectively.

**Table 5.1 Dimensions of unit cell micro channel**

$W_w(\mu m)$	$W_{ch}(\mu m)$	$H_{w1}(\mu m)$	$H_{ch}(\mu m)$	$H_{w2}(\mu m)$
118	231	12700	713	5637

**Table 5.2 Dimensions of computational domain**

$W_w(\mu m)$	$W'_{ch}(\mu m)$ (in computational domain)	$H_{w1}(\mu m)$	$H_{ch}(\mu m)$	$H_{w2}(\mu m)$
118	115.5	12700	713	5637

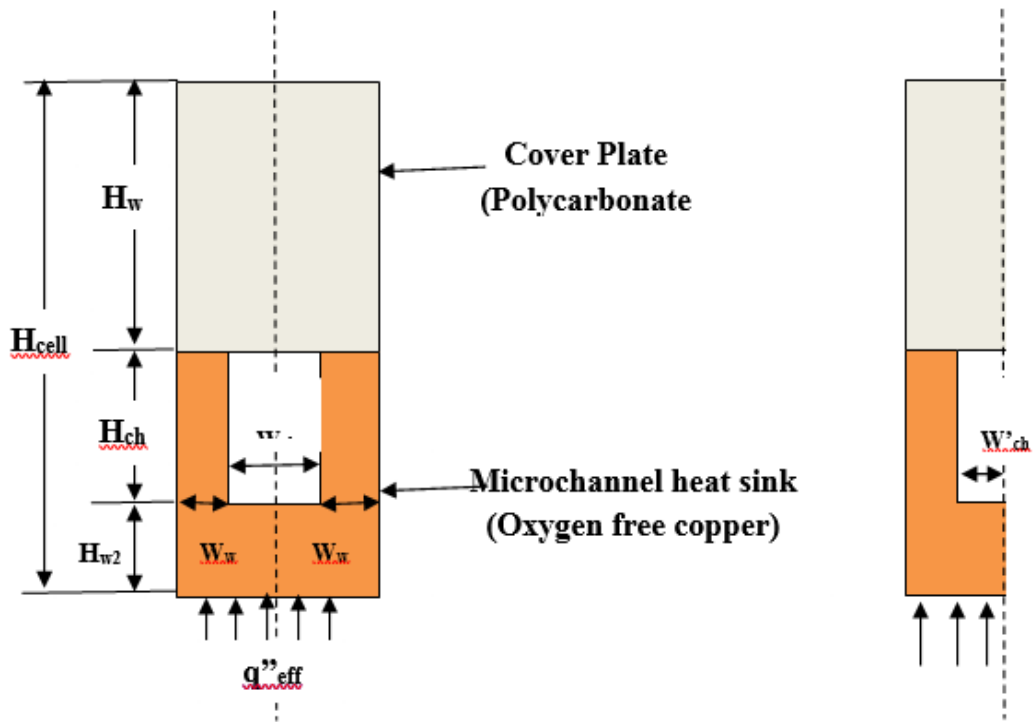


Figure 5.3 a) unit cell b) computational domain

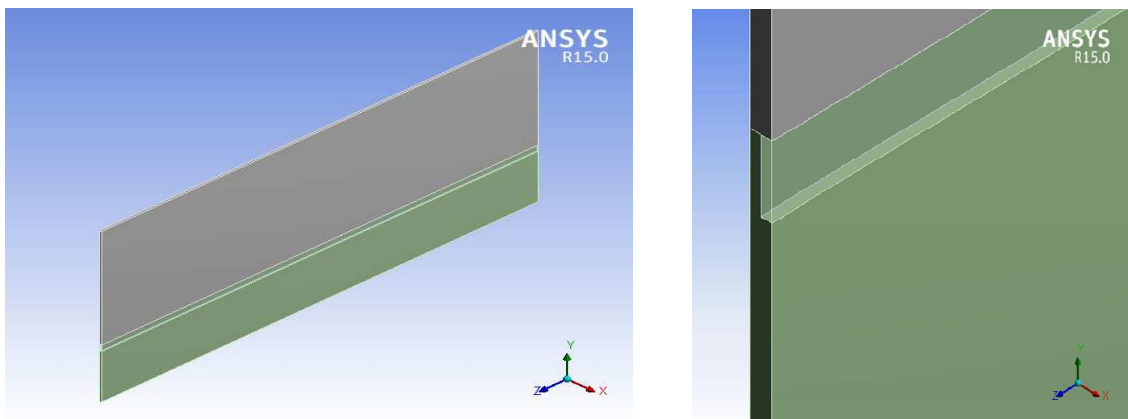


Figure 5.4 Isometric view of computational domain in ANSYS

The geometry of computational domain is prepared in solid works and heatsink bottom from outlet side is taken as origin (0,0). The length of geometry can be considered in negative  $-Z$  direction as shown in various graphs under section results and discussions.

The dimension of the entire heat sink is:

Width of Heat sink (X-direction) =  $233.5 \mu m$

Height of Heat sink (Y- direction) =  $19050 \mu m$

Length of Heat sink (Negative  $-Z$  Direction) =  $44800 \mu m$

### 5.3 Meshing of computational domain

Meshing is the most important step in any CFD analysis. The accuracy of result and time consumed during simulation work is greatly dependent upon the quality of mesh. In the current study, hexahedral mesh was used. Its detailed view is shown Fig. 5.5. Nodes and element were created using ANSYS meshing tool. The total number of mesh elements 1942320 and total number of nodes 2344509 were created. The total number of elements in fluid domain is 1020088 as it is our prime area of interest.

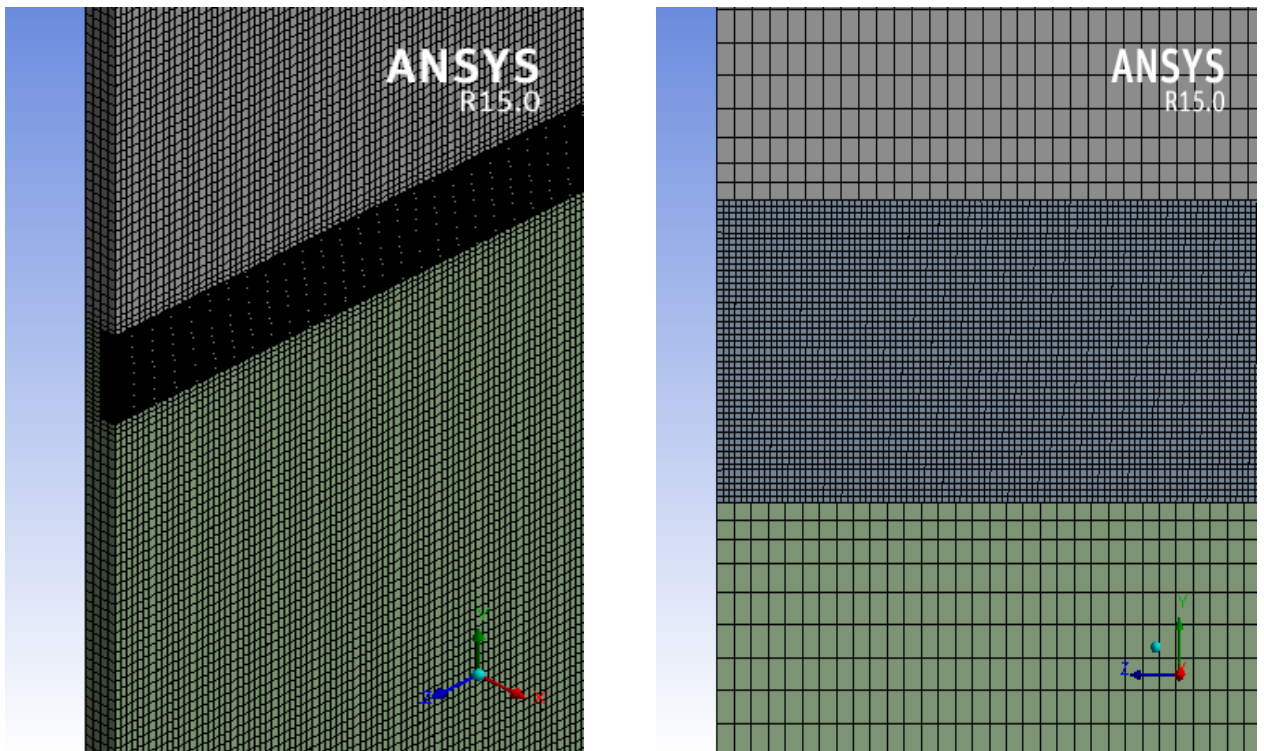


Figure 5.5 Isometric view of mesh structure in computational domain

## 5.4 Physical model

In this study, the Reynolds number  $Re = \frac{\rho u D}{\mu}$ , varies between 139-1672 which is much 2000. On the basis of the range of Reynolds number, the entire study is done with viscous laminar model keeping energy on.

## 5.5 Material properties

The properties of different material used in the present simulation work are given in table 5.3.

**Table 5.3 Material Properties**

MATERIAL	THERMAL CONDUCTIVITY, k (W/m.K)	SPECIFIC HEAT, Cp (kJ/Kg.K)
WATER	0.6	4.1855
COPPER	401	0.39
POLYCARBONATE	0.2	1.2

## 5.6 Governing Equations

The friction factor in microchannel is obtained from the pressure drop inside the channel

$$f = \frac{\Delta P_{ch} D_h}{2 L u^2 \rho_f} \quad (5.1)$$

The heat flux for single unit of microchannel is derived from equation (Qu and Mudawar 2007) [14]

$$q''_{eff} = \frac{P_w}{N A_{bot}} \quad (5.2)$$

$N$  represents no. of microchannels.  $A_{bot} = W_{cell} \times L$  (area of bottom of single microchannel).

## 5.7 Boundary conditions

The hydraulic boundary conditions are assigned as follows:

The channel inlet is assigned with a uniform velocity i.e.  $u=u_{in}$ ;  $v=0$  and  $w=0$ .

Channel inner walls: No slip

Velocity inlet: Uniform velocity and constant inlet temperature ( $T_{in}=15\text{ }^{\circ}\text{C}$ ). The velocity is calculated from the mass flow rate.

Pressure outlet: Pressure was specified. The pressure was calculated from the pressure drop inside the channel.

Thermal boundary conditions are given as follows:

At single unit cell bottom, copper wall: Constant heat flux is applied.

At the top of single unit cell, polycarbonate wall: It is subjected to convective condition where film heat transfer coefficient,  $h=10\text{ watt/m.K}$  and  $T_{amb}=25\text{ }^{\circ}\text{C}$ . All the other sink surfaces subjected to adiabatic conditions (heat flux is zero except bottom sink). The domain is designated "solid" in case of heat sink and "fluid" in case of channel. All boundary conditions as per zone is shown in the table given below.

**Table 5.4. Zone wise Boundary Condition**

ZONE	TYPE
Heat sink Inlet	Wall
Heat sink Outlet	Wall
Heat sink Bottom	Heat flux
Heat sink Top	Convection
Heat sink Left	Wall
Heat sink Right	Wall

Channel Inlet	Velocity Inlet
Channel Outlet	Pressure Outlet
Channel bottom	Wall
Channel Left	Wall
Channe Right	Wall
Channel Top	Wall

### 5.8 Method of solution

In the present simulation work, solver uses a pressure velocity coupling method SIMPLE (Semi Implicit method for Pressure Linked equation) algorithm with 2<sup>nd</sup> order upwind scheme. The convergence criteria were given  $10^{-7}$  for all parameters. The relaxation factors as per table 5.4 were used for calculations.

**Table 5.5 Relaxation factor**

<b>FACTORS</b>	<b>VALUE</b>
PRESSURE	0.3
DENSITY	1
BODY FORCE	1
MOMENTUM	0.7
ENERGY	1



## CHAPTER-6

### RESULTS AND DISCUSSIONS

The thermal behavior of the microchannel heat sink can be studied in terms of temperature distribution. The CFD analysis is carried out in two conditions at various key position of the microchannel heat sink. In first CFD analysis, the volume flow rate is 603 ml/min and the inlet velocity is 2.9056 m/sec for Reynolds number of 890. A heat flux of  $100 \text{ W/cm}^2$  is applied at the bottom of heat sink. In second condition, the volume flow rate is 585 ml/min and the inlet velocity is 2.8189 m/sec for Reynolds number of 864. A heat flux of  $200 \text{ W/cm}^2$  is applied at the bottom of heat sink. Thus the flow is laminar in both the cases.

In Fig. 6.1 and 6.11; temperature distribution along the length of bottom of heat sink is shown for  $\text{Re}=890$  at  $q_{\text{eff}}=100 \text{ W/cm}^2$  and  $\text{Re}=864$  at  $q_{\text{eff}}=200 \text{ W/cm}^2$  respectively. It can be clearly observed that the temperature is almost linearly increasing from 320 K to 337.5 K and 352.5 K to 388 K respectively in both the above cases while the inlet water temperature is fixed at 288 K. It is quite understandable that as the flow of water progresses, the temperature of water rises due to heat transfer from the bottom of heat sink to water. Due to this, the available temperature gradient reduces along the length of channel which in turn reduces the rate of heat transfer. That is why; temperature of bottom wall goes on increasing along the length of channel.

In Fig. 6.2 and 6.12; temperature distribution along the length of top of heat sink is shown at

$\text{Re}=890$  at  $q_{\text{eff}}=100 \text{ W/cm}^2$  and  $\text{Re}=864$  at  $q_{\text{eff}}=200 \text{ W/cm}^2$  respectively. It can be seen from the graph that the temperature is increasing from 300 K to 308 K and 308 K to 324 K at above conditions respectively. Such a low temperature rise owes to very low thermal conductivity of poly carbonate ( $K=0.2 \text{ W/m.K}$ ) cover which is subjected to natural convective conditions ( $h=10 \text{ W/m.K}$ ,  $T_{\text{amb}}=298 \text{ K}$ ).

In Fig. 6.3 and 6.13; temperature distribution is shown along the length of bottom wall of microchannel at  $Re= 890$  at  $q_{eff} =100 \text{ W/cm}^2$  and  $Re=864$  at  $q_{eff} =200 \text{ W/cm}^2$  respectively. The graphs show the temperature variation along the complete bottom wall surface of microchannel. The temperature of water rises from 288 K at inlet to 325 K and 288 K to 362 K at the outlet of channel, in both the above conditions respectively. The water temperature rise along the flow direction is due to the constant heat flux applied at the bottom of heat sink. As the flow of water progresses, the temperature of water rises due to heat transfer from the bottom of heat sink to water. Due to this, the available temperature gradient keeps on reducing along the length of channel which in turn reduces the rate of heat transfer and raises the temperature of water towards the outlet of channel continuously.

In Fig. 6.4 and 6.14; temperature distribution is shown along the length of complete side wall of microchannel at  $Re= 890$  at  $q_{eff} =100 \text{ W/cm}^2$  and  $Re=864$  at  $q_{eff} =200 \text{ W/cm}^2$  respectively. The temperature of water rises from 288 K at inlet to 325 K and 288 K to 362 K at the outlet of channel, in both the above condition respectively. The reason for the temperature rise of water is same as in case of bottom wall of microchannel.

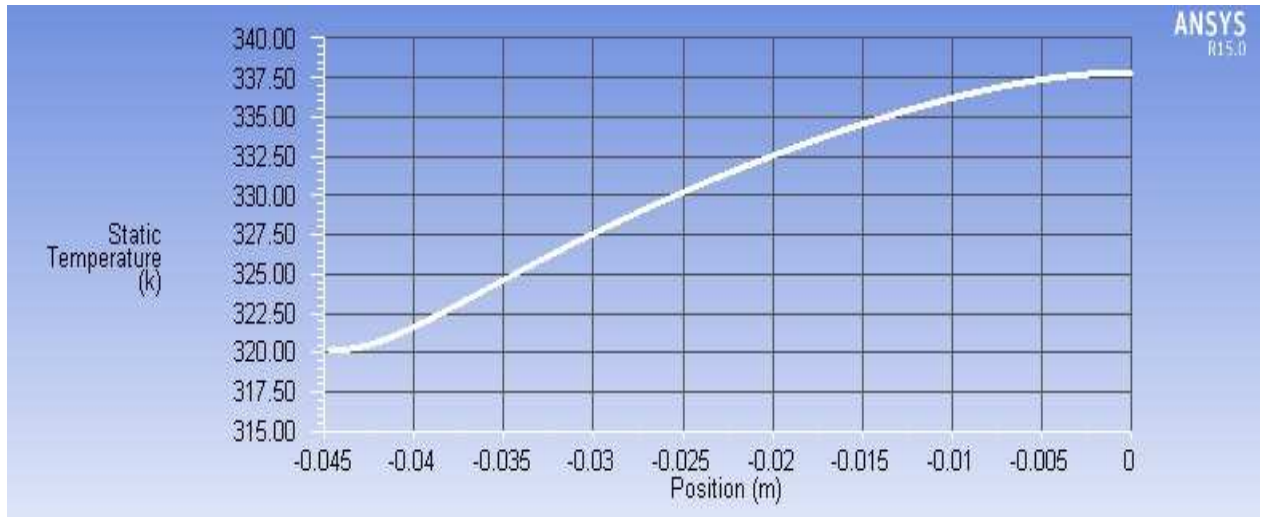
In Fig. 6.5 and 6.15; velocity contours are shown in complete fluid domain of microchannel at  $Re= 890$  at  $q_{eff} =100 \text{ W/cm}^2$  and  $Re=864$  at  $q_{eff} =200 \text{ W/cm}^2$  respectively. It can be clearly observed that the maximum velocity is at the center of the channel flow. In Fig. 6.6 and 6.16; velocity contours are shown in the area which is nearer to the inlet of microchannel at above conditions respectively. As the flow progresses, the growth of boundary layer can be clearly observed until the flow is fully hydrodynamically developed. It can also be observed from the Fig. 6.6 and 6.16; that the entrance length is becoming higher with the rise in Reynolds number. In Fig. 6.7 and 6.17; velocity contours are shown in the area which is nearer to the outlet of microchannel at above conditions respectively. It can be seen that flow is fully developed at the outlet of microchannel having maximum velocity at the center of microchannel.

In Fig.6.8 and 6.18; pressure contours is shown in the area which is nearer to the inlet of microchannel at  $Re= 890$  at  $q_{\text{eff}} =100 \text{ W/cm}^2$  and  $Re=864$  at  $q_{\text{eff}} =200 \text{ W/cm}^2$  respectively. It shows that the pressure keeps on decreasing linearly in the flow direction. This pressure drop is due to the friction which is directly proportional to pressure drop [equation-4.1]. In Fig. 6.9 and 6.19; pressure contours is shown in the area which is nearer to the outlet of microchannel at above conditions respectively. The increase in pressure drop, with increase in Reynolds number is also shown in Fig. 6.21 (both, experimental and numerical). Fig. 6.21 shows good similarity between the experimental and computed pressure drops. For a fluid with constant properties flowing through a rectangular channel, one would expect a linear relationship between pressure drop and Reynolds number. There are several reasons for the slope change in the pressure drop characteristics in Fig.6.21. First, for constant power input and water inlet temperature, the outlet water temperature should decrease with increasing Reynolds number as shown in Fig. 6.22. This in turn increases water viscosity, resulting in a larger pressure drop. Second, the inlet and outlet pressure losses are proportional to the square of velocity. Therefore, the increment in Reynolds number generates a greater effect in the inlet and outlet pressure losses.

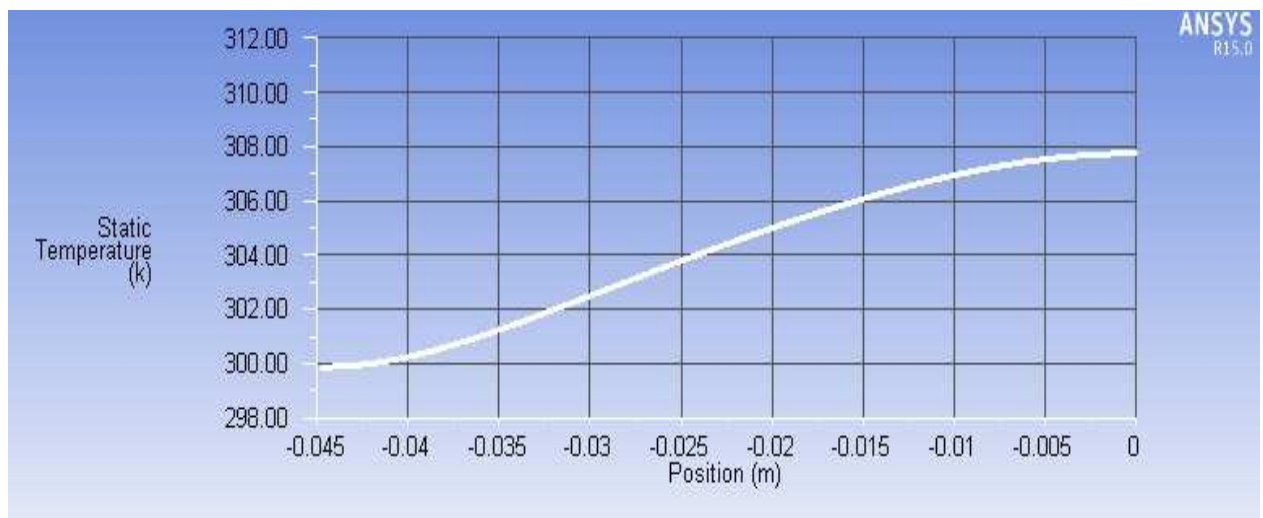
Fig. 6.22 gives the comparison between the experimental values of rise in temperature between the channel inlet and outlet, and theoretical values obtained from the energy balance

$$\rho_f \dot{V} c_{p,f} (T_{\text{out}} - T_{\text{in}}) = P_w. \quad 6.1$$

In Fig. 6.10 and 6.20; the contours of temperature variation in complete heat sink at middle plane is shown for  $Re= 890$  at  $q_{\text{eff}} =100 \text{ W/cm}^2$  and  $Re=864$  at  $q_{\text{eff}} =200 \text{ W/cm}^2$  respectively. It shows that the highest temperature is encountered in the bottom wall of heat sink below the channel outlet and lowest temperature is obtained immediately below the channel inlet.

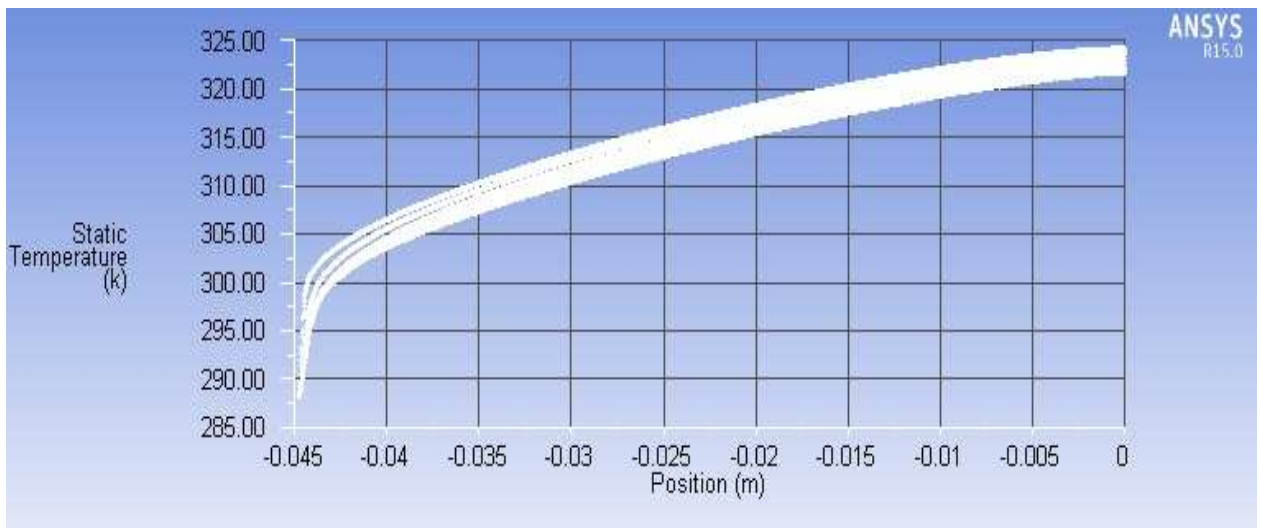


*\*Figure 6.1 Temperature distribution at bottom wall of Heat sink at  $q_{eff} = 100 \text{ W/cm}^2$  and  $Re$  of 890*

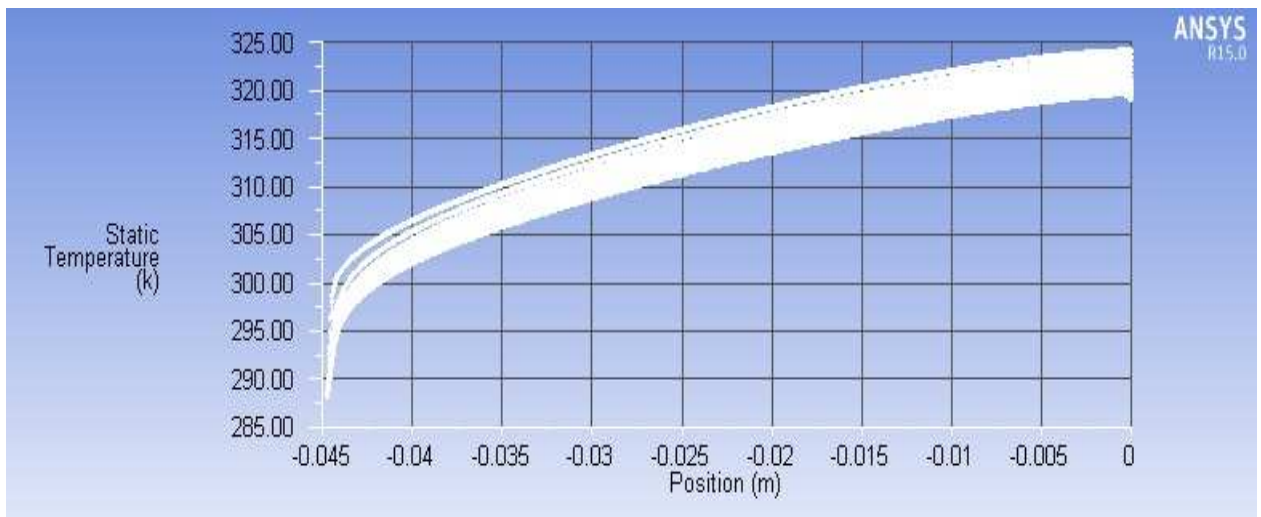


*\*Figure 6.2 Temperature distribution at Top wall of Heat sink at  $q_{eff} = 100 \text{ W/cm}^2$  and  $Re$  of 890*

*\*The graph is started from negative values due to the reason that outlet of heat sink is assigned as origin i.e. zero point. The length of heat sink is 0.0448 m so graph starts from negative sign (-0.045 m)*

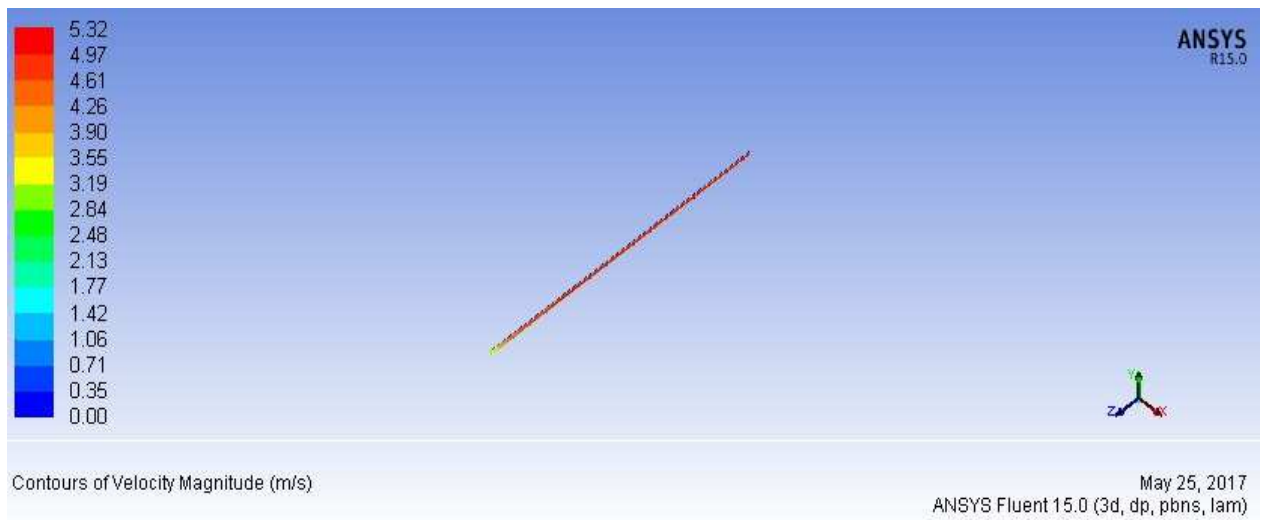


*\*Figure 6.3 Temperature distribution at Channel bottom wall of Heat sink at  $q_{eff} = 100 \text{ W/cm}^2$  and  $Re$  of 890*

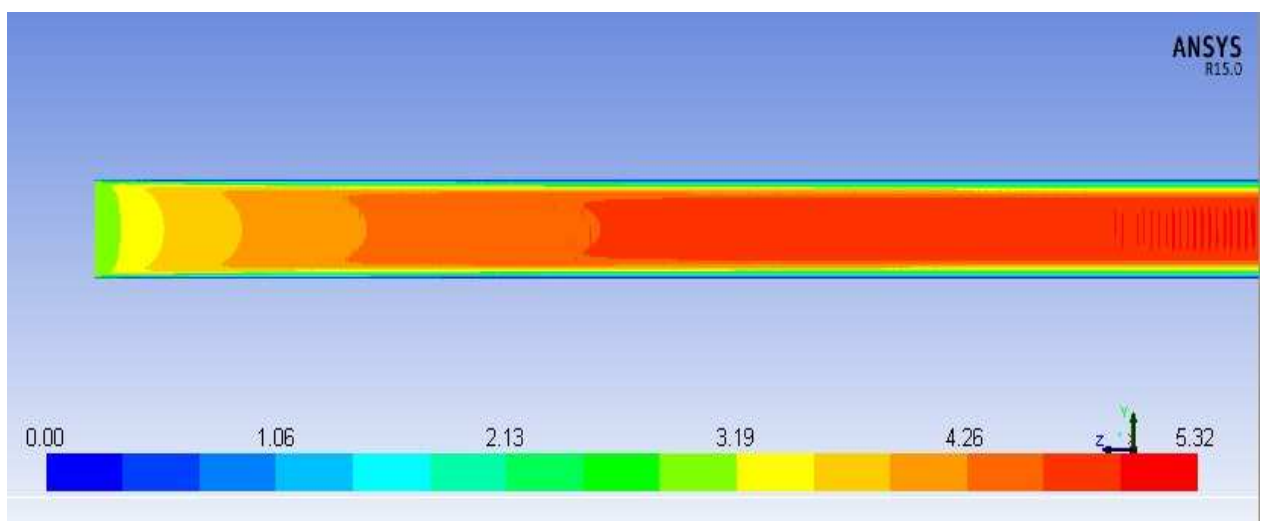


*\*Figure 6.4 Temperature distribution at Channel side wall of Heat sink at  $q_{eff} = 100 \text{ W/cm}^2$  and  $Re$  of 890*

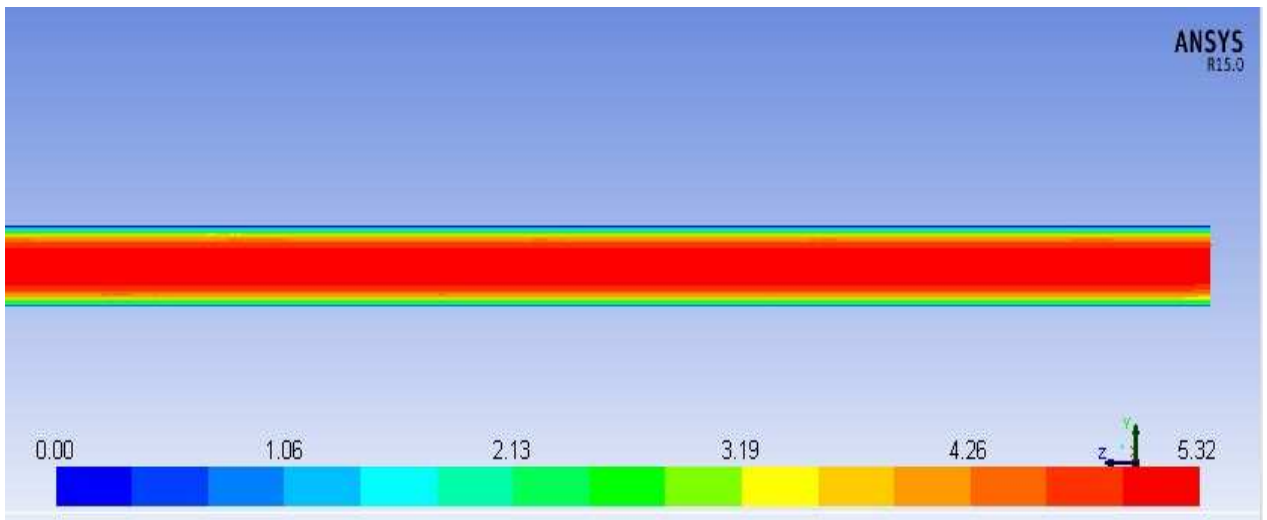
\*The graph is started from negative values due to the reason that outlet of heat sink is assigned as origin i.e. zero point. The length of heat sink is 0.0448 m so graph starts from negative sign (-0.045 m)



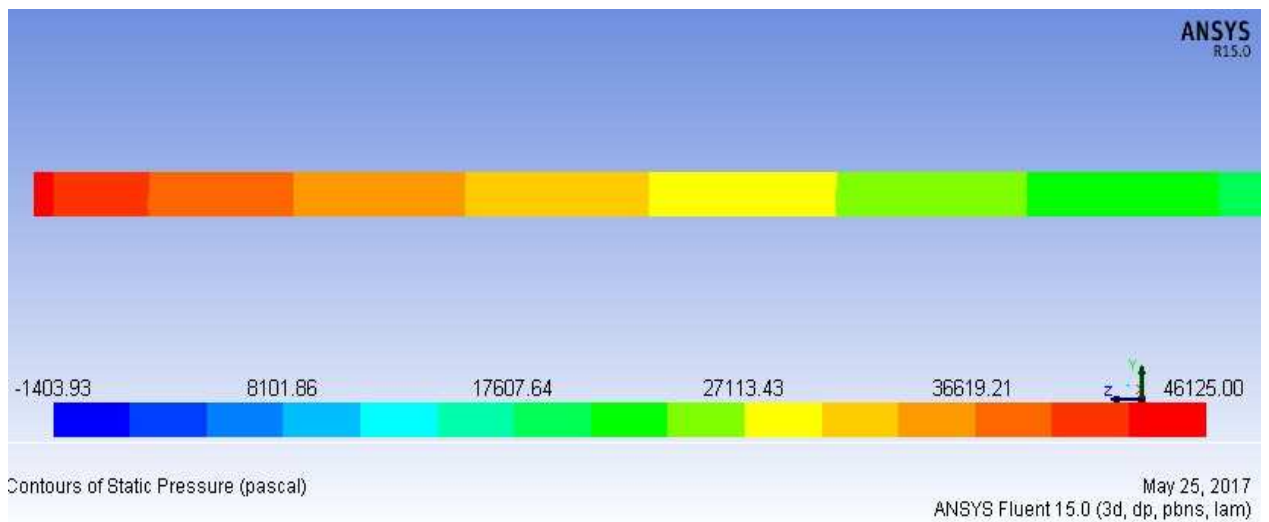
*Figure 6.5 Velocity contours in complete fluid domain at  $q_{eff} = 100 \text{ W/cm}^2$  and  $Re$  of 890*



*Figure 6.6 Velocity contours nearer to inlet at  $q_{eff} = 100 \text{ W/cm}^2$  and  $Re$  of 890*



*Figure 6.7 Velocity contours nearer to outlet at  $q_{eff} = 100 \text{ W/cm}^2$  and  $Re$  of 890*



*Figure 6.8 Pressure contours nearer to inlet at  $q_{eff} = 100 \text{ W/cm}^2$  and  $Re$  of 890*

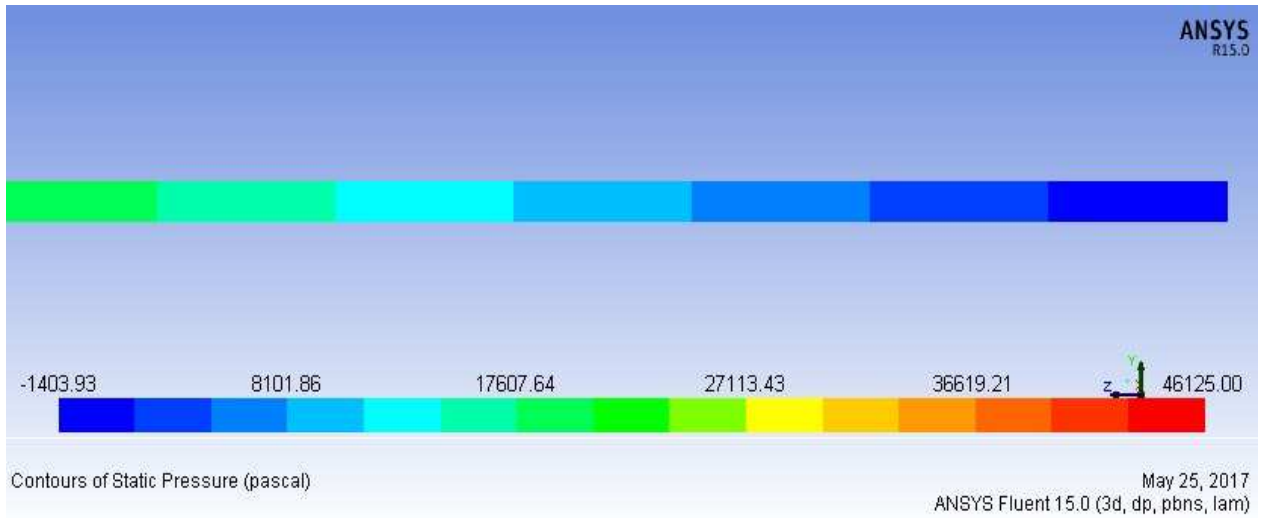


Figure 6.9 Pressure contours nearer to outlet at  $q_{eff} = 100 \text{ W/cm}^2$  and  $Re$  of 890

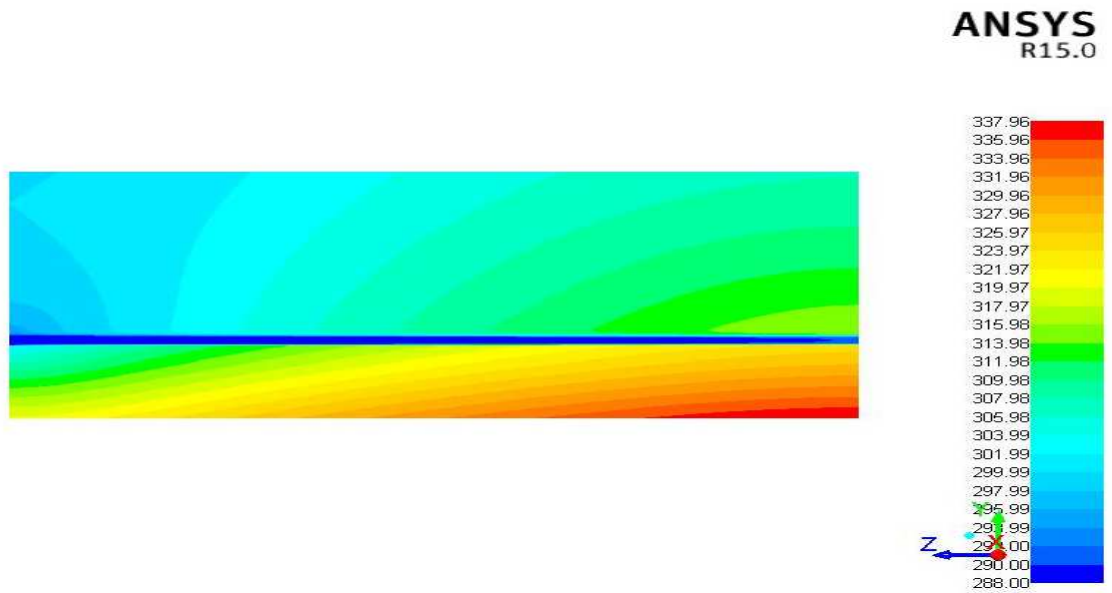
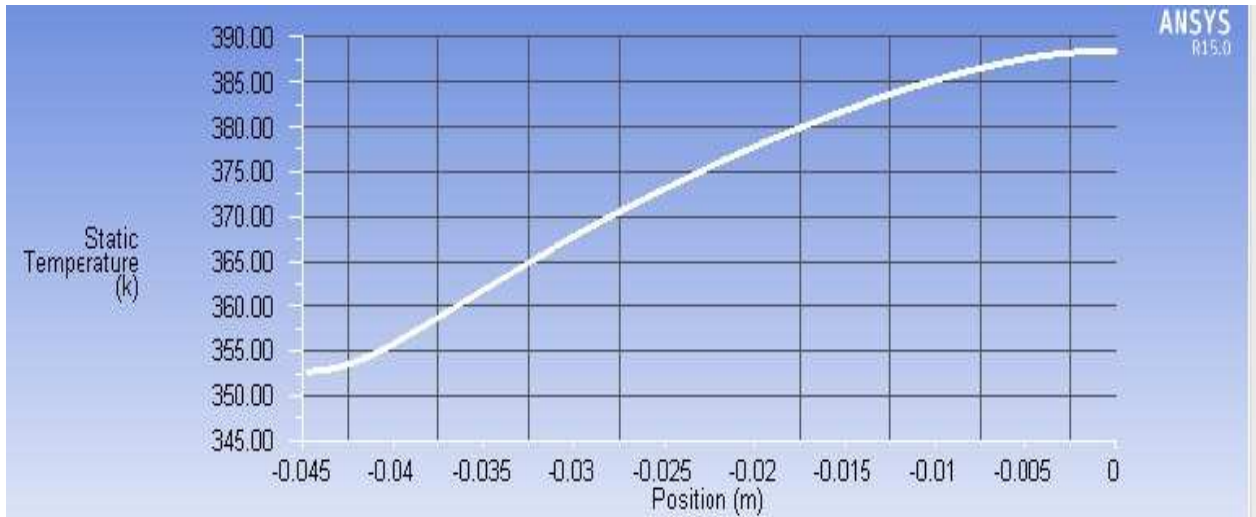
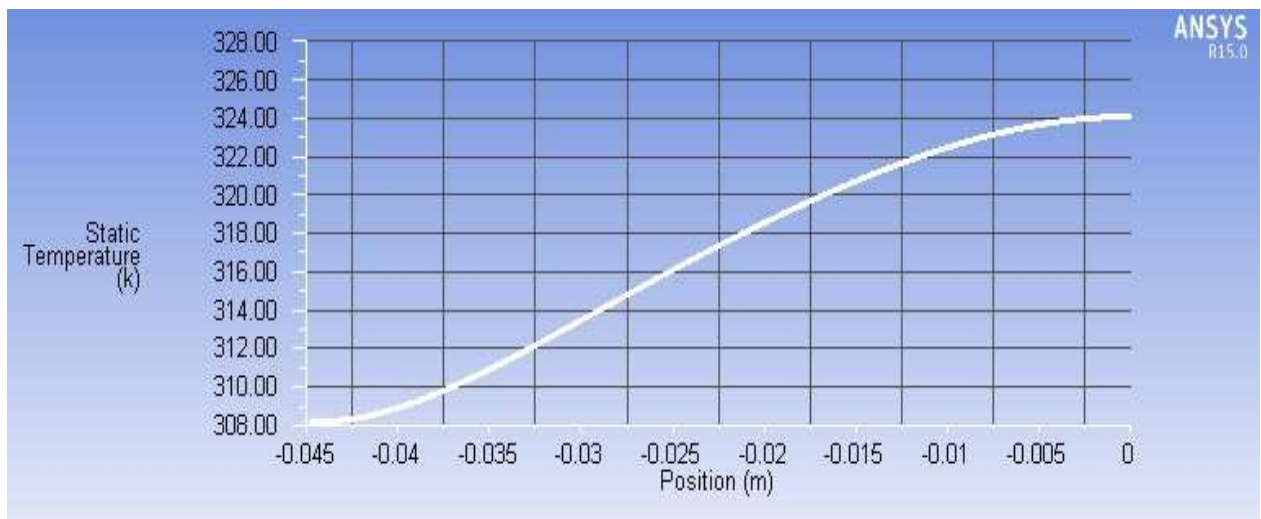


Figure 6.10 Temperature contours of complete heat sink at symmetry plane at  $q_{eff} = 100 \text{ W/cm}^2$  and  $Re$  of 890



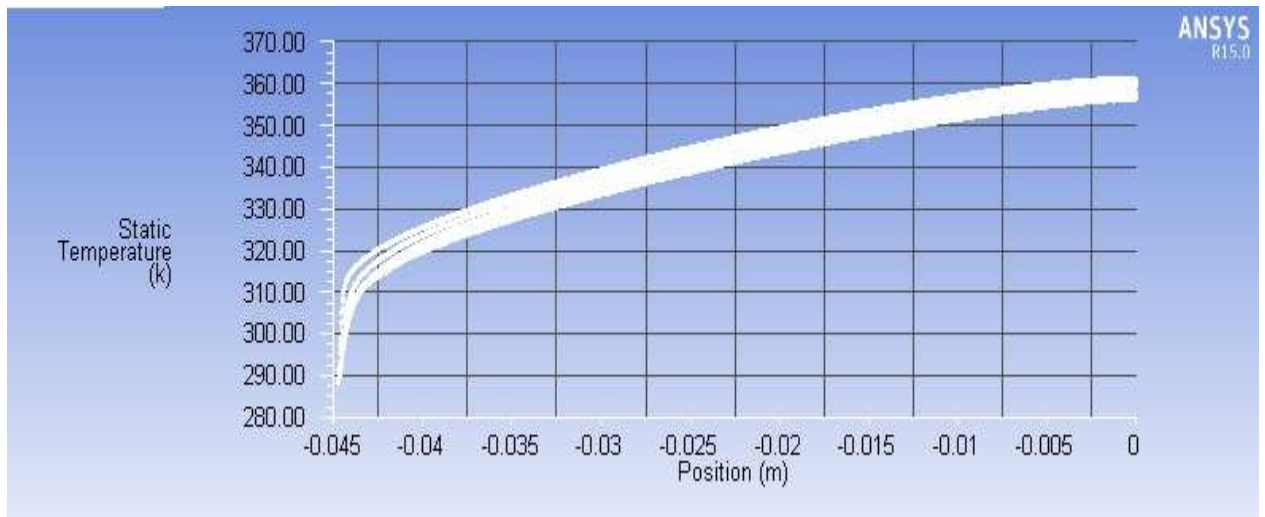


*\*Figure 6.11 Temperature distributions at bottom wall of Heat sink at  $q_{eff} = 200 \text{ W/cm}^2$  and  $Re$  of 864*



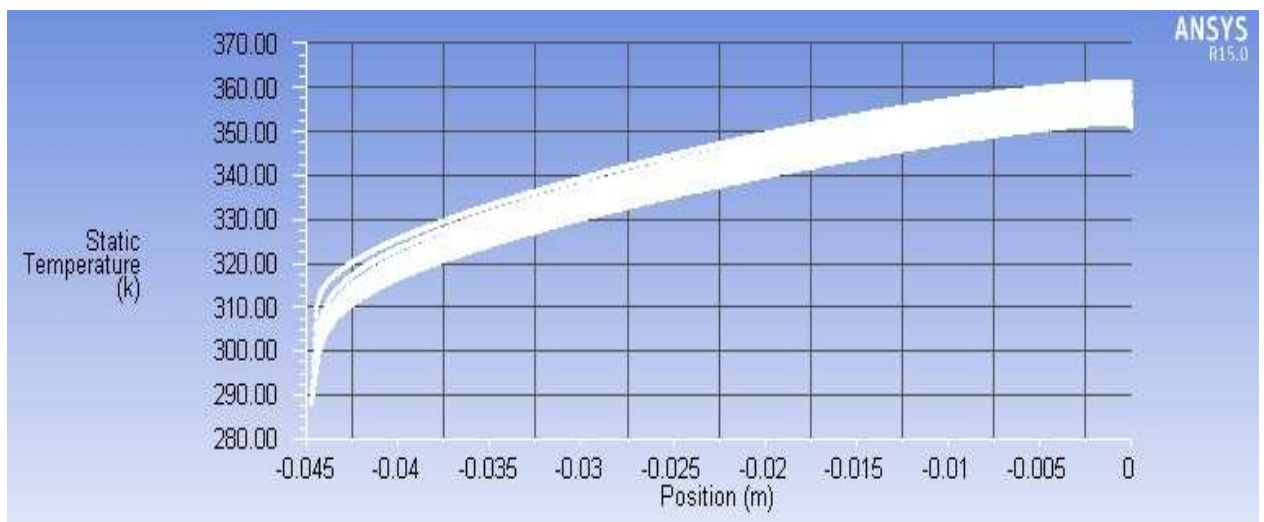
*\*Figure 6.12 Temperature distributions at top wall of Heat sink at  $q_{eff} = 200 \text{ W/cm}^2$  and  $Re$  of 864*

*\*The graph is started from negative values due to the reason that outlet of heat sink is assigned as origin i.e. zero point. The length of heat sink is 0.0448 m so graph starts from negative sign (-0.045 m)*



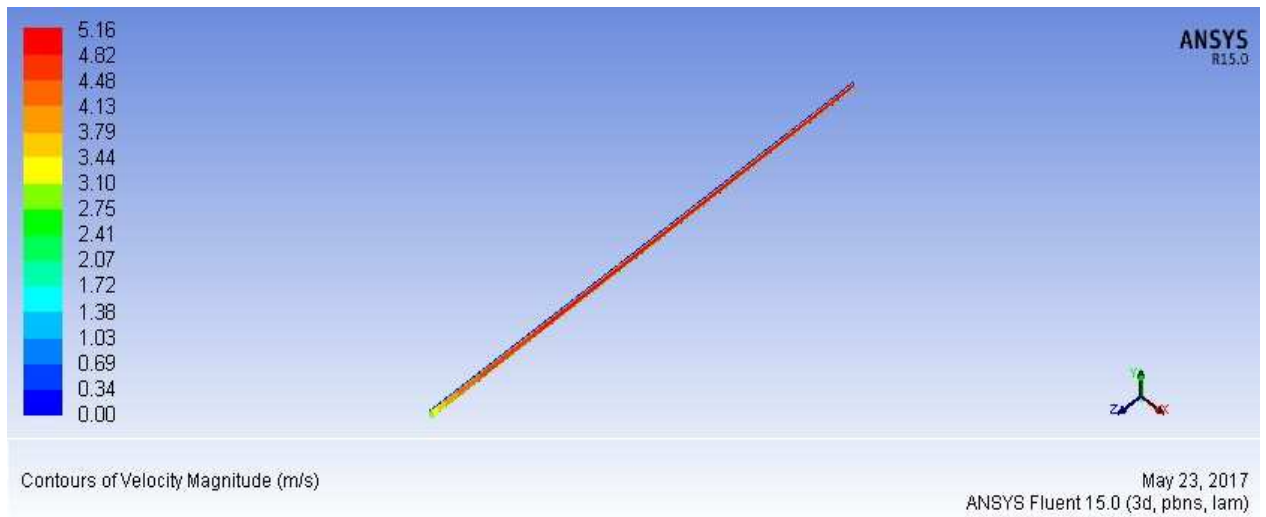
*\*Figure 6.13 Temperature distribution at Channel bottom wall of Heat sink at  $q_{eff} = 200 \text{ W/cm}^2$  and  $Re$  of 864*

zz

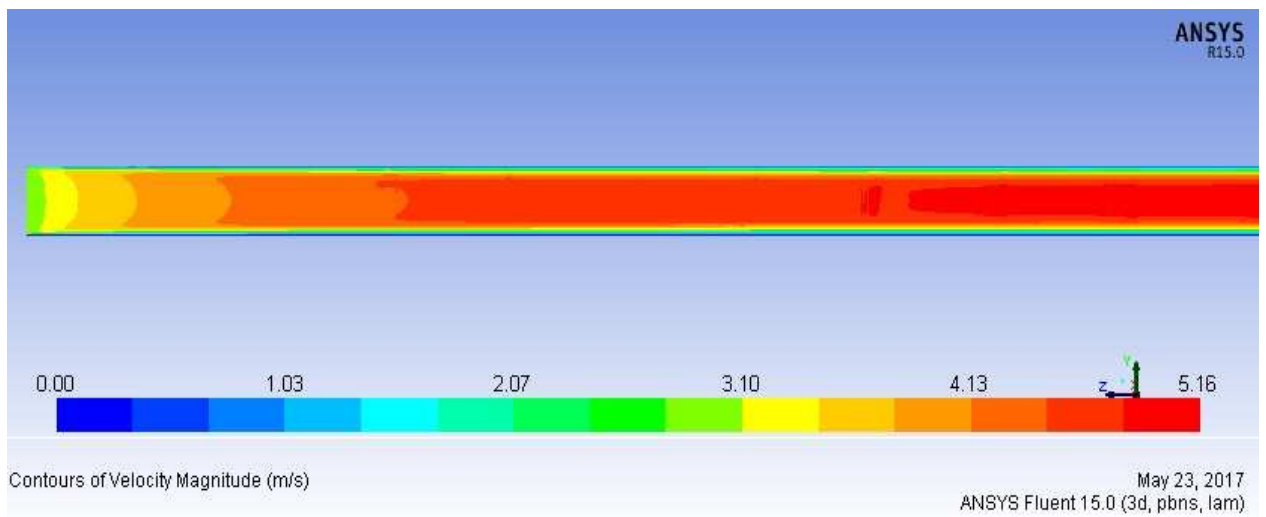


*\*Figure 6.14 Temperature distribution at Channel side wall of Heat sink at  $q_{eff} = 200 \text{ W/cm}^2$  and  $Re$  of 864*

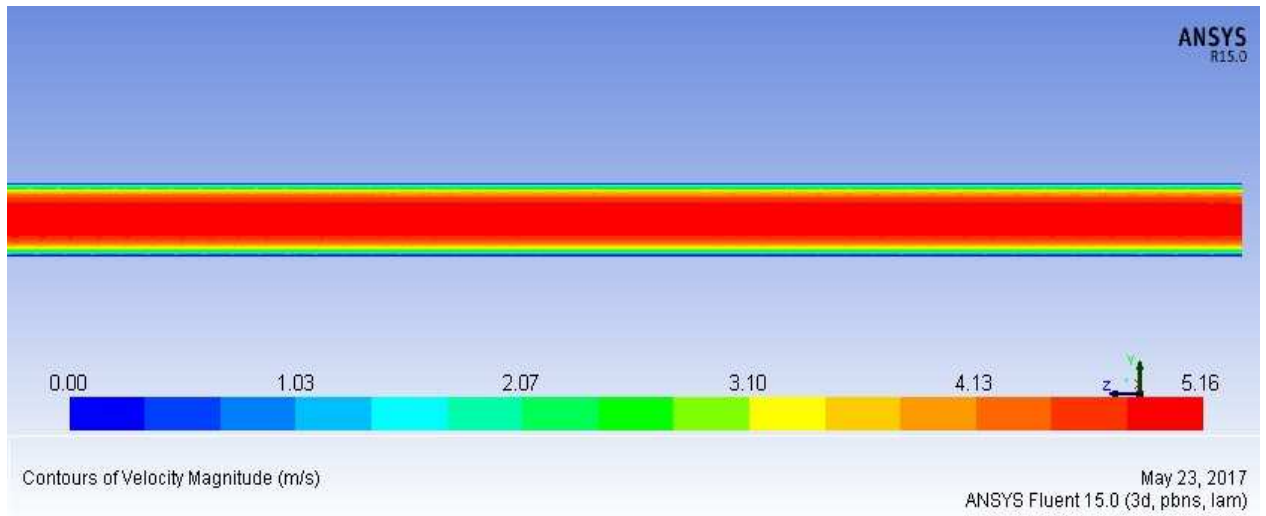
*\*The graph is started from negative values due to the reason that outlet of heat sink is assigned as origin i.e. zero point. The length of heat sink is 0.0448 m so graph starts from negative sign (-0.045 m)*



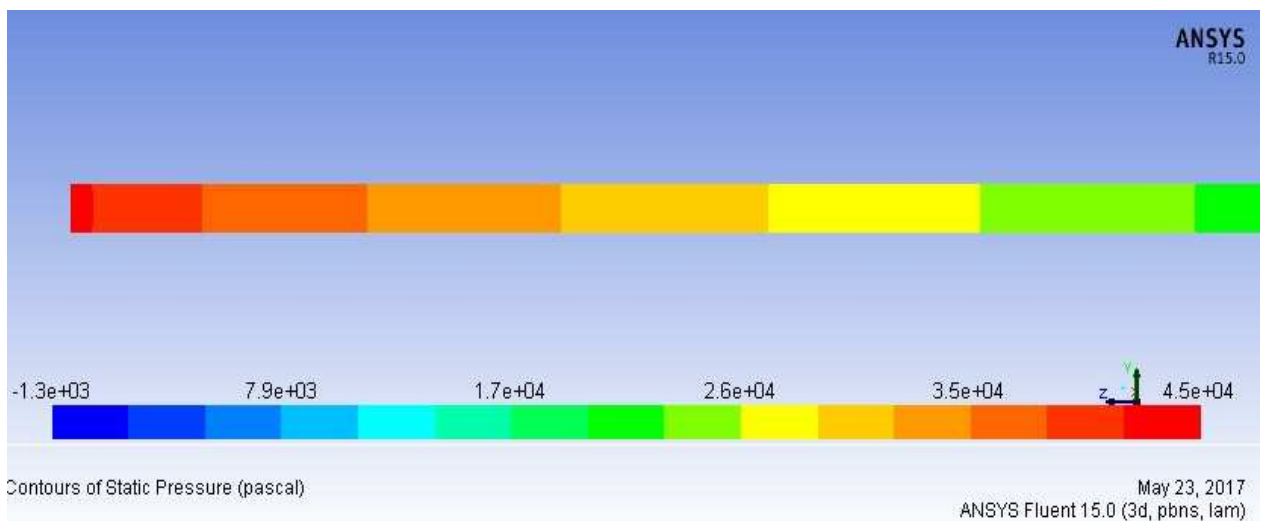
*Figure 6.15 Velocity contours in entire fluid domain at  $q_{eff} = 200 \text{ W/cm}^2$  and  $Re$  of 864*



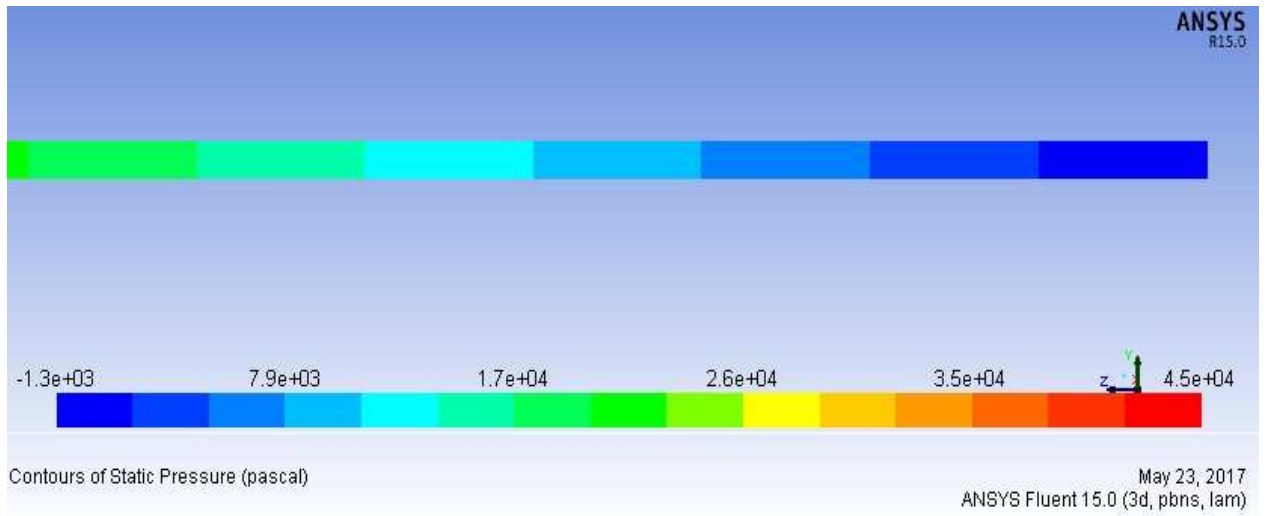
*Figure 6.16 Velocity contours nearer to inlet at  $q_{eff} = 200 \text{ W/cm}^2$  and  $Re$  of 864*



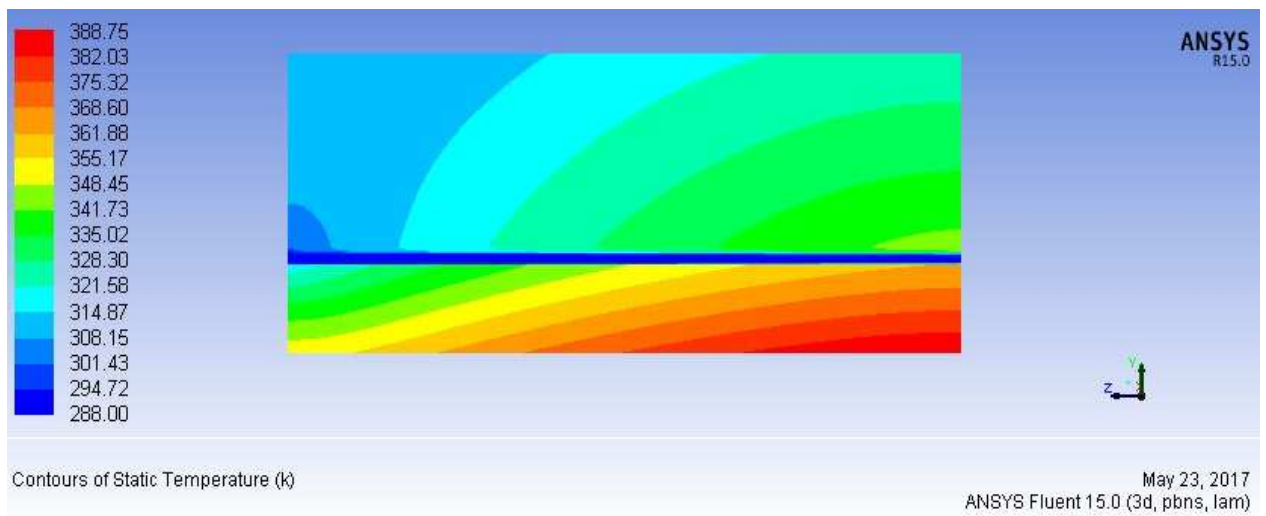
*Figure 6.17 Velocity contours nearer to inlet at  $q_{eff} = 200 \text{ W/cm}^2$  and  $Re$  of 864*



*Figure 6.18 Pressure contours nearer to inlet at  $q_{eff} = 200 \text{ W/cm}^2$  and  $Re$  of 864*



*Figure 6.19 Pressure contours nearer to inlet at  $q_{eff} = 200 \text{ W/cm}^2$  and  $Re$  of 864*



*Figure 6.20 Temperature contours of complete heat sink at symmetry plane at  $q_{eff} = 200 \text{ W/cm}^2$  and  $Re$  of 864*

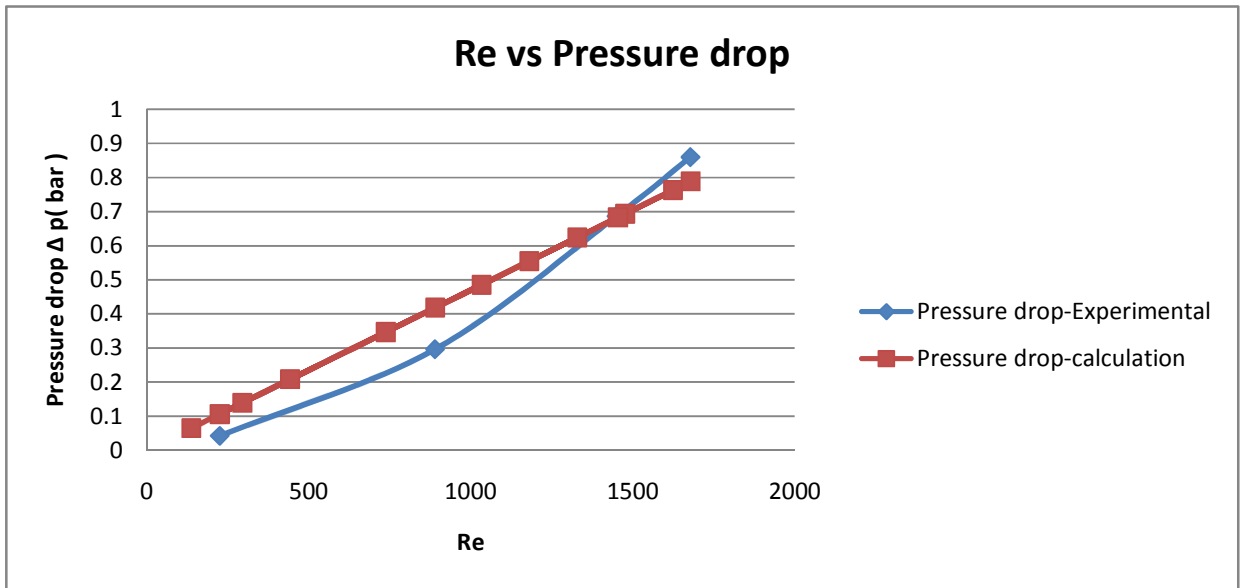


Figure 6.21 Graph between Pressure drop and Reynolds Number

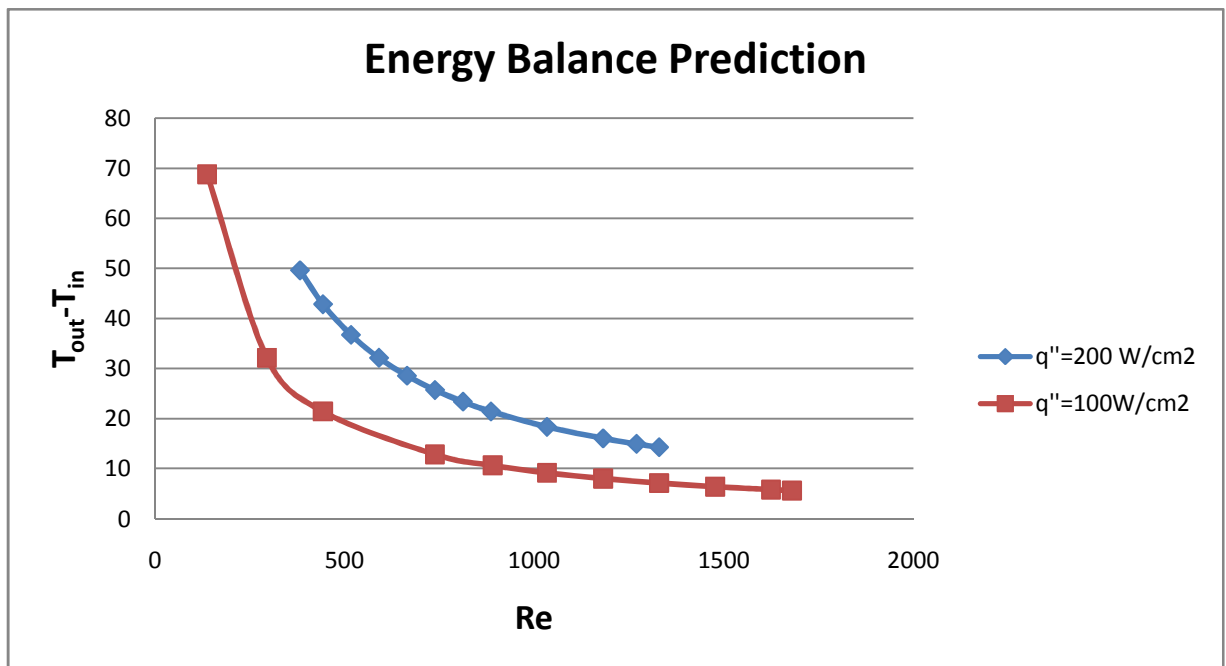
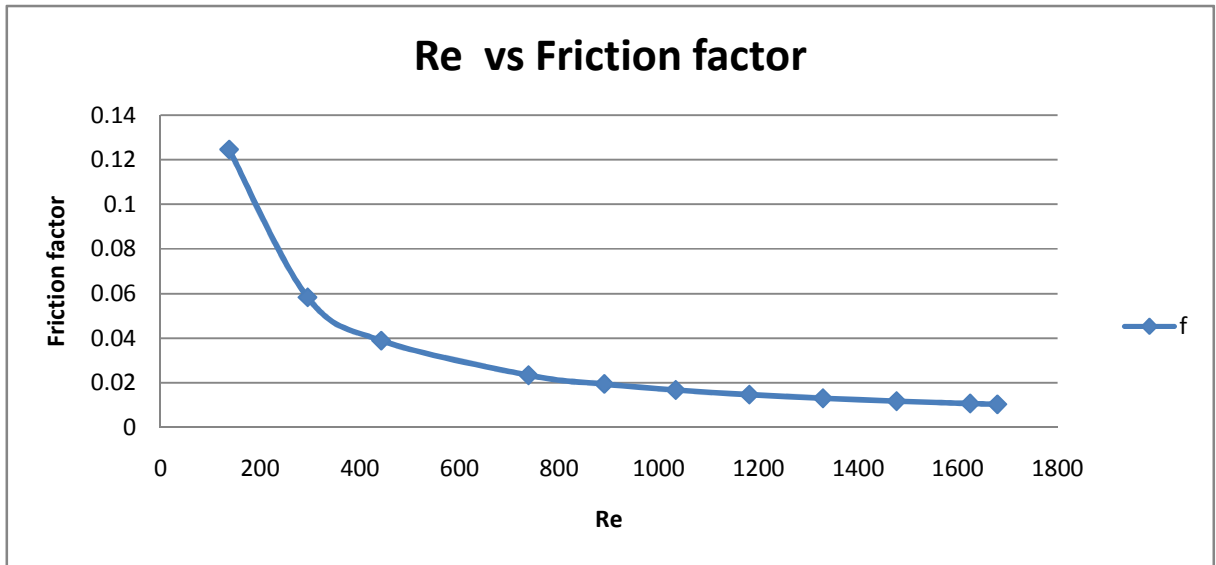


Figure 6.22 energy balance predictions for water temperature rise from heat sink inlet to outlet:  
 (a)  $q_{eff} = 100 \text{ W/cm}^2$ , (b)  $q_{eff} = 200 \text{ W/cm}^2$ .



*Figure 6.23 Graph between friction factor and Reynolds Number*

## CHAPTER -7

### CONCLUSIONS

In this study, the hydrodynamic and heat exchange analysis of rectangular microchannel in a test rig was studied. A steady state condition and laminar flow conditions were simulated by ANSYS Fluent 15.0 for the CFD analysis. Based on the above analysis; these conclusions can be drawn:

- The computed variation in temperature along heat sink walls and pressure drop inside channel can quite accurately predict the experimental results.
- A good agreement was obtained between the experimental data and results from CFD analysis for the temperature distribution within the heat sink and channel walls. Wall temperature increases in almost linear fashion from the entry of microchannel to the exit of microchannel.
- Temperature contours, pressure contours and velocity contours successfully show the hydrodynamic and thermal nature of the heat sink.
- Higher Reynolds numbers are beneficial at reducing both the water outlet temperature and the temperatures within the heat sink, at the expense of greater pressure drop.
- The highest temperature is encountered in the bottom wall of heat sink below the channel outlet and lowest temperature is obtained immediately below the channel inlet.



## REFERENCES

- [1] Advanced Materials for Thermal Management of Electronic Packaging, By Xingcun Colin Tong . Page-6,2011.
- [2]R. J. Phillips, L. R. Glicksman, and R. Larson, Forced-Convection, Liquid Cooled, Microchannel Heat Sinks for High Power-Density Microelectronics, in: *Proc.Int. Symp. on Cooling Technology for Electronic Equipment*, Honolulu, Hawaii,pp. 295–316, 1987.
- [3]D.B. Tuckerman and R. F. W. Pease, High-Performance Heat Sinking for VLSI,*IEEE Electron. Device Lett.*, Vol. EDL-2, pp. 126–129, 1981.
- [4]Mehendale, S. S., Jacobi, A.M. and Shah, R. K. 2000. Fluid Flow and Heat Transfer at Micro- and Meso-scales with Application to Heat Exchanger Design. *Applied Mechanics Reviews*, 53, 175-193.
- [5]Satish G. Kandlikar, MICROCHANNELS AND MINCHANNELS – HISTORY, TERMINOLOGY, CLASSIFICATION AND CURRENT RESEARCH NEEDS, *First International Conference on Microchannels and Minichannels April 24-25, 2003*, Rochester, New York, USA.
- [6] Obot, N.T. 2003. Toward a Better Understanding of Friction and Heat/Mass Transfer In Microchannels – A Literature Review. *Microscale Thermophysical Engineering*. 6, 155-173. 2003.
- [7] Bahrami, M and Jovanovich, M. M. 2006. Pressure Drop of Fully Developed Laminar Flow in Microchannels of Arbitrary Cross-Section. *Journal of Fluids Engineering*. 128,1036-1044.
- [8] Bayraktar, T. and Pidugu, S.B. 2006, Characterization of Liquid Flows in microfluidic Systems. *International Journal of Heat and Mass Transfer*. 49, 815-824.
- [9] Peng, X. F., Wang, B. X., Peterson, G. P., and Ma, H. B. 1995. Experimental investigation of heat transfers in flat plates with rectangular micro channels. *International Journal of Heat and Mass Transfer*. 38,127-137.
- [10] Peng, X.F. and Peterson, G.P., 1996. Convective heat transfers and flow friction for water flow in micro channel structures. *Int. J. Heat Mass Transfer*. 39 12, 2599–2608.

- [11] Fedorov, A. G. and Raymond, V. 2000. Three-dimensional conjugate heat transfers in The micro channel heat sink for electronic packaging. *International Journal of Heat and Mass Transfer*. 43 399-415.
- [12] Kawano, K., Minakami, K., Iwasaki, H. and Ishizuka, M. 1998. Micro channel heat exchanger for cooling electrical equipment. *Appl. Heat Transfer Equip., Syst. Educ. ASME HTD-361-3/PID-3*, 173-180.
- [13] Jiang, P., Fan, M., Si, G. and Ren, Z. 2001. Thermal-hydraulic performance of small scale micro-channel and porous-media heat-exchangers. *International Journal of Heat and Mass Transfer*, 44, 1039-1051
- [14] Qu, W. and Mudawar, I. 2002. Experimental and numerical study of pressure drop and heat transfer in a single-phase micro-channel heat sink. *International Journal of Heat and Mass Transfer*. 45, 2549 – 2565
- [15] Qu, W. and Mudawar, I. 2004. Measurement and correlation of critical heat flux in two phase micro-channel heat sinks. *International Journal Heat Mass Transfer*. 47, 2045–2059.
- [16] Mishan, Y., Mosyak, A., Pogrebnyak, E. and Hetsroni, G. 2007. Effect of developing flow and thermal regime on momentum and heat transfer in micro-scale heat sink *International Journal of Heat and Mass Transfer*. 50, 3100 – 3114.
- [17] Lee, J. and Mudawar, I. 2007. Assessment of the effectiveness of nanofluids for singlephase and two-phase heat transfer in micro-channels. *International Journal of Heat and Mass Transfer*. 50, 452 – 463.
- [18] Chein, R. and Chuang, J. 2007. Experimental microchannel heat sink performance studies using nanofluids. *International Journal of Thermal Sciences*. 46, 57-66.
- [19] Jung, J., Oh, H. and Kwak, H. 2009. Forced convective heat transfer of nanofluids in microchannels. *International Journal of Heat and Mass Transfer*. 52, 466 – 472.
- [20] Ergu, O. B., Sara, O.N., Yapıcı, S. and Arzutug, S. 2009. Pressure drop and point mass transfer in a rectangular microchannel. *International Communications in Heat and Mass Transfer*. 36. 618 – 623.
- [21] Liu, D. and Garimella, S.V. 2004, Investigation of liquid flow in micro channels, *AIAA J. Thermo phys. Heat Transfer* 18, 65–72.

- [22] Li, J., Peterson, G.P. and Cheng, P. 2004. Three-dimensional analysis of heat transfer in a micro-heat sink with single phase flow. *International Journal of Heat and Mass Transfer*. 47, 4215–4231.
- [23] Roy, G., Nguyen, C. T. and Lajoie, P. 2004. Numerical investigation of laminar flow and heat transfer in a radial flow cooling system with the use of nanofluids. *Superlattices and Microstructures*. 35, 497 – 511.
- [24] Roy, G., Nguyen, C. T. and Lajoie, P. 2004. Numerical investigation of laminar flow and heat transfer in a radial flow cooling system with the use of nanofluids. *Superlattices and Microstructures*. 35, 497 – 511
- [25] Hetsroni , G., Mosyak, A., Pogrebnyak, E. and Yarin, L.P. 2005. Fluid flow in microchannels. *International Journal of Heat and Mass Transfer*. 48, 1982–1998.
- [26] Khanafer, K., Vafai, K. and Lightstone, M. 2003. Buoyancy-driven heat transfer enhancement in a two-dimensional enclosure utilizing nanofluids. *International Journal of Heat and Mass Transfer*. 46, 3639–3653.
- [27] Jou, R. and Tzeng, S. 2006. Numerical research of nature convective heat transfer enhancement filled with nanofluids in rectangular enclosures. *International Communications in Heat and Mass Transfer*. 33, 727-736.
- [28] Li, C. H. and Peterson, G. P. 2007. Mixing effect on the enhancement of the effective thermal conductivity of nanoparticle suspensions (nanofluids). *International Journal of Heat and Mass Transfer*. 50, 4668 – 4677.
- [29] Xu, J.L. and Song, Y.X. 2008. Numerical simulations of interrupted and conventional micro channel heat sinks. *International Journal in Heat and Mass Transfer*. 51, 5906– 5917.
- [30] Sabbah, R., Farid, M. M. and Al-Hallaj, S. 2008. Micro-channel heat sink with slurry of water with micro-encapsulated phase change material: 3D-numerical study. *Int. J. Applied Thermal Engineering*. 29, 445–454.
- [31] Oztop, H. F. and Abu-Nada, E. 2008. Numerical study of natural convection in partially heated rectangular enclosures filled with nanofluids. *International Journal of Heat and Fluid Flow*. 29, 1326–1336.

- [32] Mokrani, O., Bourouga, B., Castelain, C. and Peerhossaini, H. 2009. Fluid flow and convective heat transfer in flat micro channels. *International Journal of Heat and Mass Transfer*. 52, 1337–1352
- [33] Muthamilselvan, M., Kandaswamy, P. and Lee, J. 2009. Heat transfer enhancement of copper-water nanofluids in a lid-driven enclosure. *Commun Nonlinear Sci Numer Simulat*. 5(7), 28 – 44
- [34] Al-Nimr, M.A., Maqableh, M., Khadrawi, A.F. and. Ammourah, S.A. 2009. Fully developed thermal behaviors for parallel flow microchannel heat exchanger, *International Communications in Heat and Mass Transfer*. 36, 385-390.
- [35] Mathew, B. and Hegab, H. 2009. Application of effectiveness-NTU relationship to parallel flow microchannel heat exchangers subjected to external heat transfer. *International Journal of Thermal Sciences*. 30, 1-10
- [36] Kang, S. and Tseng, S. 2007. Analysis of effectiveness and pressure drop in micro crossflow heat exchanger, *Applied Thermal Engineering*. 27, 877-885.
- [37] Tsuzuki, N., Utamura, M. and Ngo, T. 2009. Nusselt number correlations for a microchannel heat exchanger hot water supplier with S-shaped fins, *Applied Thermal Engineering*, 29, 3299-3308
- [38] Evgeny, V., Rebrov, N., Jaap, Schouten, C. and Croon, M. 2011, Single-phase fluid flow distribution and heat transfer in micro structured reactors. *Chemical Engineering Science*. 66 1374–1393
- [39] Bachok, N., Ishak, A. and Pop, I. 2011. Flow and heat transfer over a rotating porous disk in a nanofluid. *Physica B*. 406, 1767 – 1772.
- [40] Allen, P. W. 2007. Experimental and Numerical Investigation of Fluid Flow and Heat Transfer in Microchannels. Msc Thesis, Mechanical Engineering Department, Louisiana State University.
- [41] B.B. Arora, “CFD Analysis of Angle Axial Annular Diffuser with Both Hub and Casing at Diverging Equal Angles”, *International Journal of Advanced Production and Industrial Engineering*, IJAPIE-2016-01-109, Vol 1(1), PP. 33-38.
- [42] Aditya Rastogi, Siddharth Arora, B. B. Arora, “Computerized Determination of Air Flow Around Airfoils and Optimization of the Design for Fulfilment of the Objective”,

International Conference of Advance Research and Innovation (ICARI-2014), ISBN 978-93-5156-328-0, PP. 575-579.

[43] B.B. Arora, "Performance Analysis of Parallel Hub Diverging Casing Axial Annular Diffuser with 20-Degree Equivalent Cone Angle", Australian Journal of Mechanical Engineering, Vol 12 No.2, 6(2014), PP. 179-194.

[44] Abhishek Goyal, Gaurav Gosain, B.B. Arora and Rakesh Kumar "Finite Element Analysis of Blind Flanges" International Journal of Theoretical and Applied Mechanics, ISSN 0973-6085 Volume 7, Number 1 (2012) PP. 77-88.

[45] Manoj Kumar, B.B. Arora, Subhashish Maji and S. Maji, "Effect of Area Ratio and Inlet Swirl On the Performance of Annular Diffuser" International Journals of Applied Engineering Research, ISSN 0973-4562, Volume 7, Number 13 (2012) PP. 1493-1506.

[46] Manoj Kumar, B.B. Arora, Subhashis Maji. S. Maji, "Effect of Equivalent Cone Angle On the Performance of Parallel Hub Diverging Casing Annular Diffuser," International Journal of Fluids Engineering. ISSN 0974-3138 Volume 4, No.2. (2012), PP. 97-104.

[47] Manoj Kumar, B.B. Arora, Subhashis Maji. S. Maji, "Effect of Inlet Swirl On the Flow Behavior Inside Annular Diffuser," International Journal of Dynamics of Fluid Volume 7, Number 2 (2011), PP. 181-188. ISSN 0973-1784

[48] B. B. Arora, B. D. Pathak, "CFD Analysis of Axial Annular Diffuser with Both Hub and Casing Diverging at Unequal Angles," International Journal of Dynamics of Fluid Vol.7, No.1. (2011), PP. 109-121, ISSN 0973-1784.

[49] B. B Arora, R. K Sharma, A. Gogoi, Vipin and J.N. Rai, "CFD Analysis of a Free Power Turbine for an Auxiliary Power Unit", International Journal of Theoretical and Applied Mechanics, Vol. 5, No. 2, 2010, PP. 223-232

[50] B.B. Arora, R.K. Sharma, A. Gogoi, Vipin and J.N. Rai, "CFD Analysis of a Free Power Turbine for an Auxiliary Power Unit," International Journal of Theoretical and Applied Mechanics, Volume 5 Number 2 (2010) PP. 223-232.

[51] B.B. Arora, Manoj Kumar, Subhashis Maji, "Study of Inlet Conditions On Diffuser Performance," International Journal of Theoretical and applied Mechanics, Vol.5, No.2. (2010), PP. 201-221, ISSN 09736085.

[52] B.B. Arora, B.D. Pathak, "Effect of Inlet Swirl On the Pressure Recovery of Annular Diffuser" International Journal of Fluids Engineering, ISSN 0974-3138 Volume 2, Number 3 (2009), PP. 201-209.